

# RESEARCH ACTIVITIES VIII

## Computer Center

### VIII-A Theoretical Studies on Electronic Structure and Dynamics of Electronically Excited States in Polyatomic Molecules

#### VIII-A-1 Theoretical Study on the Spectroscopy and Dynamics of Electronically Excited States of HCP Molecule

NANBU, Shinkoh; KINOSHITA, Tomoko; GRAY, Stephen K.<sup>1</sup>; AOYAGI, Mutsumi  
(<sup>1</sup>Argonne Natl. Lab.)

Quantum mechanical bound-state calculations for the low-lying electronic excited states of HCP molecule,  $1^1A''$ ,  $2^1A'$  and  $2^1A''$ , were performed using the ab initio global potential energy surfaces. The global potential surfaces were determined by the multi-reference configuration interaction (MRCI) method at DZP basis set level. A large direct-product basis coupled with the standard Lanczos iterative method was employed for computing the rovibrational energy levels. An evenly spaced discrete variable representation (DVR) was used to describe the two radial coordinates of Jacobi coordinates, and the Gauss-Legendre quadrature points was used as an angular DVR for the bending coordinate. The results almost reproduced the low-lying vibrational levels for the  $1^1A''$  state measured in the UV absorption spectrum and IR-UV double resonance spectroscopy, and moreover the term energies of the  $1^1A''$  and  $2^1A''$  states with including the zero point vibrational energy were also in good agreement with the experimental data at aug-cc-pVDZ basis set level. We also performed wave packet calculations on ab initio surfaces to investigate the photodissociation dynamics for  $HCP(1^1\Sigma^+) + h\nu \rightarrow H(2S) + CP(X)$ ; where  $X = 1^2\Sigma^+$  and  $2^2\Pi$ . It is found that the non-adiabatic transition between  $1^1A'$  and  $2^1A'$  states in the bent conformations plays an important role in the predissociation process.

#### VIII-A-2 Development of *Ab Initio* MD Method Based on the Direct Evaluation of CAS-SCF Energy Derivatives

KINOSHITA, Tomoko; NANBU, Shinkoh; AOYAGI, Mutsumi

We have been developing an ab initio molecular dynamics programs to investigate the reaction dynamics of large scale problems, *i.e.*, surface reactions, and biological systems. Since we employed parallelized version of McMurchie-Davidson's algorithm to evaluate both AO integrals and derivatives of AO integrals, the most time consuming step of electronic structure calculations has been carried out in a tractable way. At each time steps of MD calculations, we obtain analytical energy derivatives of complete active space (CAS) wavefunctions. We continue to develop the codes for non adiabatic and spin-orbit coupling matrix elements.

Our direct method can easily extend to apply a number of interesting problems including non adiabatic reactions and spin forbidden processes.

#### VIII-A-3 Theoretical Study on the Unimolecular Reaction Dynamics of Acetyl Radical $CH_3CO \rightarrow CH_3 + CO$

ITO, Masakatsu; NANBU, Shinkoh; AOYAGI, Mutsumi

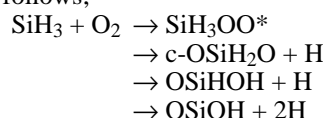
We investigate the dissociation dynamics of acetyl radical with the classical trajectory method using the electronic model hamiltonian based on our ab initio calculations. At each time step in our classical trajectory calculations, the electronic hamiltonian is diagonalized to obtain the instantaneous adiabatic states and then the Hellmann-Feynmann forces are evaluated to drive the nuclear coordinates. Our hamiltonian is based on the valence bond (VB) description of the electronic wavefunctions. Since acetyl radical and its dissociative products have different bonding characters, the wavefunctions along the dissociation process are approximately expanded by two corresponding VB bases states. We found that the energy of the CCO bending excitation does not efficiently transfer into the dissociation coordinate (C-C) over the time period of 30 ps. It is suggested that this slow transfer or redistribution of internal energy could be one of the important sources for the discrepancy between the RRKM rate constants and the experimental results.

#### VIII-A-4 *Ab Initio* Molecular Orbital Studies of Isomerization Reaction from *c*-OSiH<sub>2</sub>O to *t*-OSiHOH

KONDO, Shigeo<sup>1</sup>; TOKUHASHI, Kazuaki<sup>1</sup>; NAGAI, Hidekazu<sup>1</sup>; TAKAHASHI, Akifumi<sup>1</sup>; SUGIE, Masaaki<sup>1</sup>; AOYAGI, Mutsumi  
(<sup>1</sup>Natl. Inst. Mater. Chem. Res.)

[*J. Mol. Struct. (THEOCHEM)* **469**, 25 (1999)]

We have suggested in a previous study that the reaction route from  $SiH_3 + O_2$  to  $OSiOH + 2H$  is a key to understand the spontaneous ignition at room temperature. The whole route of this reaction was found as follows;



In this study, the isomerization reaction from *c*-OSiH<sub>2</sub>O to *t*-OSiHOH, a vital reaction to understand the

spontaneous ignition of Silane, has been reinvestigated with Gaussian-2 theory and CAS(6,6) method. It was found that the reaction proceeds through two consecutive steps; *i.e.*, *c*-OSiH<sub>2</sub>O undergoes isomerization to yield *w*-OSiH<sub>2</sub>O, and then the latter is converted to *t*-OSiHOH. The G-2 energy of the transition state of the latter process is 4.3 kcal/mol higher than that of the former. However, the G-2 energy of this higher transition state plus H atom is still 4.8 kcal/mol lower than that of the original reactants of SiH<sub>3</sub> + O<sub>2</sub>.

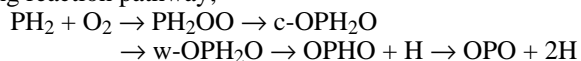
#### VIII-A-5 *Ab Initio* Study of PH<sub>2</sub> + O<sub>2</sub> Reaction Relevant to the PH<sub>3</sub> Combustion

KONDO, Shigeo<sup>1</sup>; TOKUHASHI, Kazuaki<sup>1</sup>; TAKAHASHI, Akifumi<sup>1</sup>; SUGIE, Masaaki<sup>1</sup>; AOYAGI, Mutsumi

(<sup>1</sup>Natl. Inst. Mater. Chem. Res.)

[*J. Phys. Chem. A* in press]

*Ab initio* calculations have been carried out for the PH<sub>2</sub> + O<sub>2</sub> reaction by using Gaussian-2 theory, which is considered as a key reaction to understand low temperature phosphine combustion. This reaction consists of two main branching routes at low temperatures. One is the reaction to yield OH radicals, and the other to yield hydrogen atoms. Of the two reactions, we found that a long reaction pathway;



has been concluded to be the chain branching process, which enables the spontaneous ignition of phosphine at room temperature.

#### VIII-A-6 Semiclassical Study of Nonintegrable Systems

TAKAMI, Toshiya

We study nonadiabatic processes in highly excited states of molecules. Although a lot of theoretical works have been published on the subject so far, many of the authors have considered the problem under assumption that avoided crossings are sufficiently small. In the highly excited states, however, the assumption is not always validated. A new approach is desirable in order to study dynamical processes in systems with many levels interacting each other.

Our approach for the problem starts from studying systems with boundaries in the parameter space. We showed that the transition probability in adiabatic limit is dominated by an extra transition on the boundaries, which comes from nonadiabatic couplings between adiabatic states. We also found an iterative method to define a new base in which the extra transition is suppressed and the transition by avoided crossings can be observed locally. The new base can be used to analyze nonadiabatic processes of not only two level systems but also many level ones.

Our final goal is to construct a new framework for investigating many level nonadiabatic transition in realistic systems by using the new base instead of the usual adiabatic or diabatic base, as well as to develop

the higher order asymptotic theories in nonintegrable dynamical systems.

#### VIII-A-7 A Theoretical Study on Structures and Vibrational Spectra of C<sub>84</sub> Fullerene Isomers

NISHIKAWA, Takeshi; KINOSHITA, Tomoko; NANBU, Shinkoh; AOYAGI, Mutsumi

[*J. Mol. Struct. (THEOCHEM)* 461-462, 453 (1999)]

The C<sub>2</sub>, D<sub>2</sub>, and D<sub>2d</sub> isomers of C<sub>84</sub> fullerene were investigated by *ab initio* molecular orbital calculations. Optimized geometries, relative stabilities, and vibrational spectra of eleven isomers are determined by restricted Hartree-Fock (RHF) calculations with STO-3G, 3-21G, and D95V basis sets. For the purpose of an assignment on the C<sub>84</sub> structures, we discussed a way to distinguish a specific isomer by comparing the calculated vibrational spectra.

We found that the peaks located at higher than 1300 cm<sup>-1</sup> are all belonging to the on-surface mode where each carbon atom moves on the surface of C<sub>84</sub> skeleton. On the other hand, the peaks below 1000 cm<sup>-1</sup> correspond to the breathing mode, in which atoms are moving perpendicularly to the surface. There exists a window region (around 1000–1300 cm<sup>-1</sup>) in all calculated spectra, which split a character of normal mode vibrations. In D<sub>2</sub> symmetry, the vibrational spectra of isomer No. 1 has a noticeable difference in the locations of three main peaks. The isomer No. 2 with C<sub>2</sub> symmetry also has characteristic vibrational structure, where numbering scheme introduced by Fowler *et al.* is used. For the rest of other isomers examined, it was hard to clearly predict the structure solely with calculated vibrational spectra. We suggested that the difference in the bands around 650 cm<sup>-1</sup> and 1670 cm<sup>-1</sup> can be used as a finger print of D<sub>2</sub> isomers, and that the vibrational bands below 900 cm<sup>-1</sup> and peak around 1880 cm<sup>-1</sup> can be used to distinguish C<sub>2</sub> species.

# Laser Research Center for Molecular Science

## VIII-B Developments of Advanced Lasers for Chemical Reaction Controls and ZEKE Photoelectron Spectroscopy

### VIII-B-1 Developments of Liquid Crystal Spatial Light Modulator

SATO, Shin-ichiro; WATANABE, Kazuo

The chemical reaction controls with laser lights are one of the most important subjects of chemistry. The coherence of laser lights has not been considered seriously in the old fashion of the laser controls of chemical reactions. Recent theoretical studies have shown that the more sophisticated controls of chemical reactions. As a first step, we are trying to maximize efficiency of the quantum transition with a chirped ultra short pulsed laser. This technique is based on an adiabatic passage theory of quantum transitions. We are developing a photo waveform shaper of ultra short laser pulses to make an arbitrary shaped pulse, including chirped ones. The spectral components of the incident pulse are spatially dispersed with a grating, modulated or retarded with a liquid crystal array on the Fourier plane and recombined with another grating.

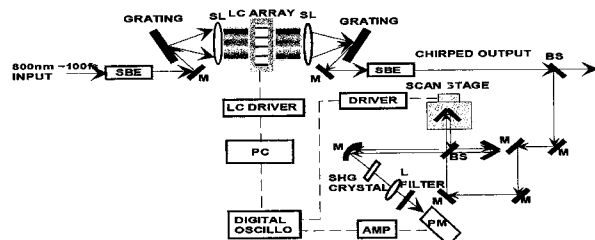


**Figure 1.** Schematic diagram of liquid crystal spatial light modulator.

### VIII-B-2 ZEKE Electron Spectroscopy of Azulene and Azulene-Argon

TANAKA, Daisaku; SATO, Shin-ichiro; KIMURA, Katsumi

Mass-selected ion-current spectra and zero-kinetic-energy (ZEKE) electron spectra were obtained for azulene and its van der Waals (vdW) complex with Ar in supersonic jets by two-photon ( $1 + 1'$ ) resonant ionization through the second singlet electronic excited state ( $S_2$ ). Ab initio calculations were also carried out to study the optimized geometry and vibrational modes for azulene in the neutral and cation ground states ( $S_0$  and  $D_0$ ). Lennard Jones (LJ) potential energy calculations including "charge-charge-induced-dipole interactions" were also made for azulene-Ar. The main results may be summarized as follows. (1) The adiabatic ionization energies have been determined as  $I_a$  (azulene) =  $59781 \pm 5 \text{ cm}^{-1}$  and  $I_a$  (azulene-Ar) =  $59708 \pm 5 \text{ cm}^{-1}$ . The difference in  $I_a$  is  $73 \text{ cm}^{-1}$ . (2) Several vibrational frequencies of (azulene)<sup>+</sup> have been observed and identified on the basis of ab initio theoretical calculations. (3)

vibrational progression with a spacing of  $9\text{--}10 \text{ cm}^{-1}$  in the ZEKE spectra of azulene-Ar has been assigned experimentally and theoretically to the vdW bending vibration  $b_x^{+1}$  along the long axis of azulene. (4) From the calculated LJ potential energy minima, it has been found that Ar is shifted by  $0.10 \text{ \AA}$  along the long axis of azulene from the position in the neutral ground state. (5) The observed vdW vibrational progressions have been reproduced by Franck-Condon calculations, suggesting that Ar is shifted by  $2^\circ$  for (azulene-Ar)<sup>+</sup> with respect to its neutral  $S_2$  state.

## VIII-C Developments and Researches of New Laser Materials

Although development of lasers is remarkable, there are no lasers which lase in ultraviolet and far infrared regions. However, it is expected that these kinds of lasers break out a great revolution in not only the molecular science but also in the industrial world.

In this project we research characters of new materials for ultraviolet and far infrared lasers, and develop new lasers by using these laser materials.

### VIII-C-1 Intense THz Radiation from Femtosecond Laser Pulses Irradiated InAs in a Strong Magnetic Field

OHTAKE, Hideyuki; ONO, Shingo<sup>1</sup>; KAWAHATA, Eiji; LIU, Zhenlin; SARUKURA, Nobuhiko  
(<sup>1</sup>Sci. Univ. Tokyo)

Since the first observation of THz radiation from InAs surface irradiated with femtosecond laser pulses, considerable effort have been made to design an intense THz-radiation source and to understand the mechanism for generating THz radiation. However, the problem has not been solved. In this paper, we have investigated the intense THz radiation from InAs by applying a strong magnetic field up to 5 T. We compared several different geometries. Besides quadratic magnetic field dependence, we found saturation of the THz-radiation intensity around 3 T. Furthermore, the intensity decreased dramatically above 3 T. It represented that the most suitable magnetic field was 3 T to design an intense THz-radiation source. We also took spectra by a Polarizing Michelson interferometer. The spectral shapes for the different magnetic field directions were significantly different. The center frequency of these spectra shifted to lower frequency with increasing magnetic field. Through these experiments, we found the best configuration and the most suitable magnetic field to obtain an intense THz radiation for various applications such as imaging, sensing, and spectroscopy. This configuration dependence of the spectral shape and the center frequency is attributed to be the initial carrier acceleration processes modulated by a strong magnetic field.

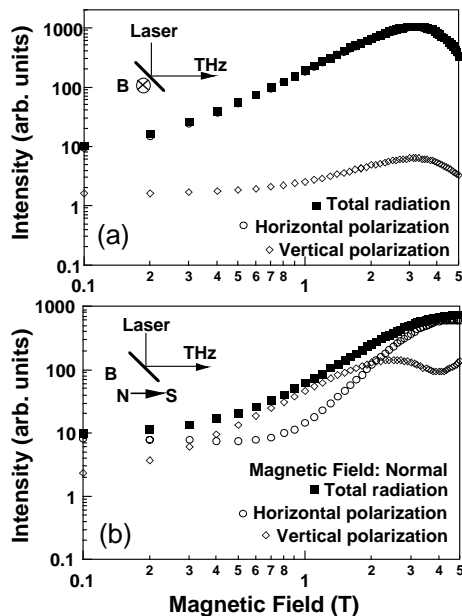


**Figure 1.** Magnetic field dependence of THz-radiation intensity. Inset indicates the experimental geometry. Closed squares, open circle and diamonds show total radiation, horizontal and vertical polarization, respectively. (a) The saturation of THz radiation intensity is clearly observed. (b) The saturation is not observed.

### VIII-C-2 High-Repetition-Rate, High-Average-Power Mode-Locked Ti:sapphire Laser with an Intracavity cw-Amplification Scheme

LIU, Zhenlin; ONO, Shingo<sup>1</sup>; KOZEKI, Toshimasa; OHTAKE, Hideyuki; SARUKURA, Nobuhiko  
(<sup>1</sup>Sci. Univ. Tokyo)

We have demonstrated a high-average-power, mode-locked Ti:sapphire laser with an intracavity cw-amplification scheme. The laser generated 150-fs pulses with 3.4-W average power at a repetition rate of 79 MHz. This simple amplification scheme can be applied for the power scaling of other lasers.

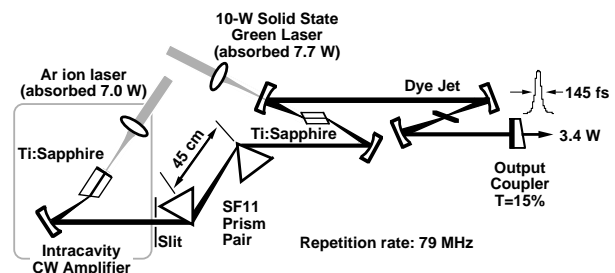


**Figure 1.** Configuration of high-repetition-rate high-average-power (3.4 W) femtosecond Ti:sapphire laser with an intracavity cw amplifier. The half-cut Brewster Ti:sapphire crystal composed the intracavity cw amplifier.

### VIII-C-3 Compact THz-radiation Source Consisting of a Bulk Semiconductor, a Mode-Locked Fiber Laser, and a 2-T Permanent Magnet

ONO, Shingo<sup>1</sup>; TSUKAMOTO, Takeyo<sup>1</sup>; KAWAHATA, Eiji; LIU, Zhenlin; OHTAKE, Hideyuki; SARUKURA, Nobuhiko; NISHIZAWA, Seizi<sup>2</sup>; NAKANISHI, Akio<sup>3</sup>; YOSHIDA, Makoto<sup>4</sup>  
(<sup>1</sup>Sci. Univ. Tokyo; <sup>2</sup>JASCO Co.; <sup>3</sup>Sumitomo Special Metals co., Ltd.; <sup>4</sup>IMRA AMERICA, INC. JLO)

Various THz-radiation sources have been intensively studied including photo conductive switches irradiated with ultrashort optical pulses. An intense, compact, and simple light source is required for applications in sensing or imaging. We have demonstrated the strong enhancement of THz-radiation power with a magnetic

field by using an InAs semiconductor. In this paper, we report on a compact THz-radiation source consisting of a fiber femtosecond laser and a newly designed 2-T permanent magnet shown in Figure 1. A mode-locked frequency doubled Er-doped fiber laser delivered 170-fsec pulses at 780 nm with a 48.5-MHz repetition rate (IMRA model FA7850/10SA) with 30-mW average power and 4.1-kW peak power. The mode-locked fiber laser is a completely turn-key system. It is much smaller than a mode-locked Ti:sapphire laser that requires daily alignment. The used semiconductor sample was undoped bulk InAs with a (100) surface. The 2-T permanent magnet unit consisted of 8 Nd-Fe-B magnet pieces. The remanence magnetic field of the Nd-Fe-B material itself was 1.3 T (NEOMAX-44H). Owing to the new magnetic circuit design, the magnetic field in the center exceeded the remanence magnetic field of the material. The permanent magnet only weighs about 5 kg. The 2-T permanent magnet unit is smaller and much lighter than an electromagnet. At present the average power is estimated to sub-micro watt level. The spectra of the THz radiation were obtained by a Polarizing Michelson interferometer. Many water vapor absorption lines were clearly observed. Therefore, the THz-radiation source is already usable for spectroscopy. Such a simple and compact source will open up new application for THz-radiation.

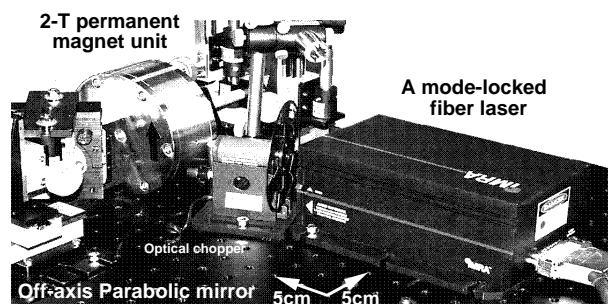


**Figure 1.** Photograph of a compact THz-radiation source with a bulk semiconductor, a fiber femtosecond laser, and a 2-T permanent magnet. Including the laser, the size is less than 40 × 30 × 15 cm.

#### VIII-C-4 Spectrum Control of THz Radiation from InAs in a Magnetic Field by Duration and Frequency Chirp of the Excitation Pulses

**KAWAHATA, Eiji; ONO, Shingo<sup>1</sup>; LIU, Zhenlin; OHTAKE, Hideyuki; SARUKURA, Nobuhiko**  
(<sup>1</sup>Sci. Univ. Tokyo)

The THz-radiation spectrum from InAs in a magnetic field irradiated with femtosecond pulses can be controlled by varying the excitation pulse width and chirp direction of the excitation pulse. A longer excitation pulse width produces lower frequency THz radiation. Also, positively chirped pulse excitation will generate higher power and higher frequency THz radiation, due to the corruption of the impulse response of the semiconductor in the longer pulse width region. The spectral shape of the radiation strongly depends on the chirp direction. This unexpected difference with the same excitation peak power and the same pulse duration

with different chirp direction is rather surprising. This difference of THz-radiation for the chirping of the excitation pulses might be attributed to the difference of the photo-carrier relaxation process in the conduction band with oppositely chirped-pulse excitation.

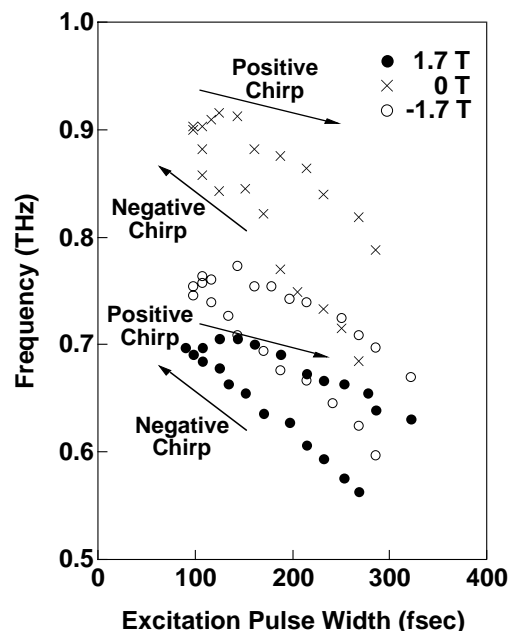


**Figure 1.** Center frequency spectrum dependence of THz radiation with different excitation chirp, pulse duration and magnetic field. Close circle, open circle and cross show 1.7 T, -1.7 T and 0 T, respectively.

#### VIII-C-5 LiCAF Crystal as a New Vacuum Ultraviolet Optical Material with Transmission down to 112 nm

**KOZEKI, Toshimasa; SAKAI, Masahiro; LIU, Zhenlin; OHTAKE, Hideyuki; SARUKURA, Nobuhiko; SEGAWA, Yusaburo<sup>1</sup>; OBA, Tomoru<sup>2</sup>; SHIMAMURA, Kiyoshi<sup>3</sup>; BALDOCHI, Sonia L.<sup>3</sup>; NAKANO, Kenji<sup>3</sup>; MUJILATU, Na<sup>3</sup>; FUKUDA, Tsuguo<sup>3</sup>**  
(<sup>1</sup>RIKEN; <sup>2</sup>Optron Inc.; <sup>3</sup>Tohoku Univ.)

LiCaAlF<sub>6</sub> (LiCAF) was found to be an ideal optical material for the vacuum ultraviolet region due to its superior transmission characteristic of down to 112 nm, its non hydroscopic nature, and its better mechanical properties compared with LiF.

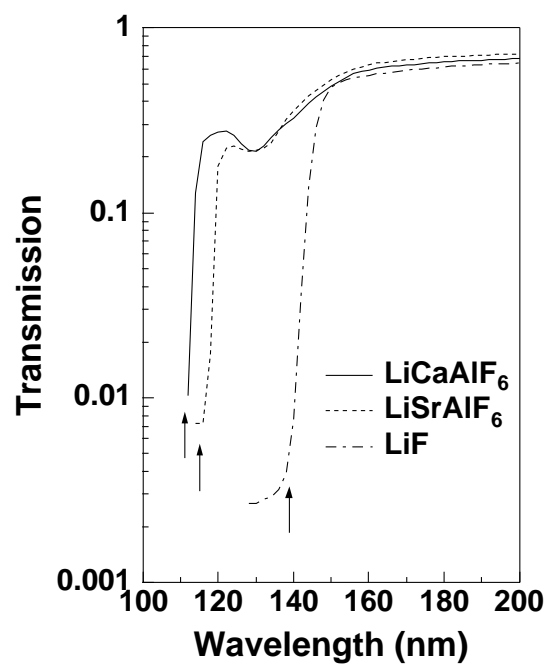


Figure 1. Transmission characteristics of LiCAF, LiSAF, LiF.

## VIII-D Development and Research of Advanced Tunable Solid State Lasers

Diode-pumped solid-state lasers can provide excellent spatial mode quality and narrow linewidths. The high spectral power brightness of these lasers has allowed high efficiency frequency extension by nonlinear frequency conversion. Moreover, the availability of new and improved nonlinear optical crystals makes these techniques more practical. Additionally, quasi phase matching (QPM) is a new technique instead of conventional birefringent phase matching for compensating phase velocity dispersion in frequency conversion. These kinds of advanced tunable solid-state light, so to speak Chroma Chip Lasers, will assist the research of molecular science.

In this projects we are developing Chroma Chip Lasers based on diode-pumped-microchip-solid-state lasers and advanced nonlinear frequency conversion technique.

### VIII-D-1 Frequency-Doubled Tunable Yb:YAG Microchip Laser for Holographic Volume Memories

SAIKAWA, Jiro; TAIRA, Takunori

Holographic volume memories have provoked a great deal of controversy.<sup>1)</sup> Angle and wavelength-multiplexed recordings have excellent potential for a large storage capacity.<sup>2,3)</sup> However, large cumbersome light sources prevent the research of holographic data storage systems. Lately, we developed diode-pumped single-frequency and tunable Yb:YAG microchip laser.<sup>4)</sup> In this work, we have demonstrated multiplex recording by using an intracavity frequency doubled Yb:YAG green laser.

The experimental configuration is shown in Figure 1. The frequency-doubled Yb:YAG laser consists of 400- $\mu\text{m}$  thickness YAG doped with 25 at.% Yb<sup>3+</sup> ion assembled on a sapphire substrate. Because the internal surface of the Yb:YAG microchip has partial reflectivity for laser wavelength, this microchip acts as an mode selection etalon. For tuning, a 1 mm thickness quartz plate was inserted into the laser cavity as a birefringent filter. A 2 mm KTP crystal was cut for type-II second-harmonic (SH) phase matching ( $\theta = 90^\circ$ ,  $\phi = 50^\circ$ ). In the frequency doubled Yb:YAG laser, tuning from 514.8 to 525.7 nm (10.9 nm, 12.4 THz) and maximum SH output power of 112 mW were obtained with single-axial-mode.

The recording medium was a 1% Fe-doped LiNbO<sub>3</sub> (Fe:LN) single crystal (3 × 3 × 5 mm). The *c*-axis of the crystal was parallel to the grating vector of the hologram. A reference beam *R* and a signal beam *S* irradiated opposite sides of the crystal, both at an angle  $\theta_0$  of 10°. A pattern mask with a 10 × 10 mm<sup>2</sup> character image, two lenses (diameter:  $d = 1\text{-inch}$ , focal length  $f = 75.5\text{-mm}$ ), the Fe:LN crystal, and a CCD camera made a Fourier-transform holographic system. We recorded and reconstructed two successive wavelength-multiplexed holograms by using light of two wavelengths that were 0.31 nm apart which corresponds to the FSR of 400- $\mu\text{m}$  Yb:YAG microchip.

#### References

- 1) J. F. Heanue *et al.*, *Science* **265**, 749 (1994).
- 2) S. Campbell and P. Yeh, *Appl. Opt.* **35**, 2380 (1996).
- 3) T. Kume *et al.*, *Jpn. J. Appl. Phys.* **35**, 448 (1996).
- 4) T. Taira *et al.*, *IEEE J. Sel. Top. Quantum Electron.* **3**, 100 (1997).

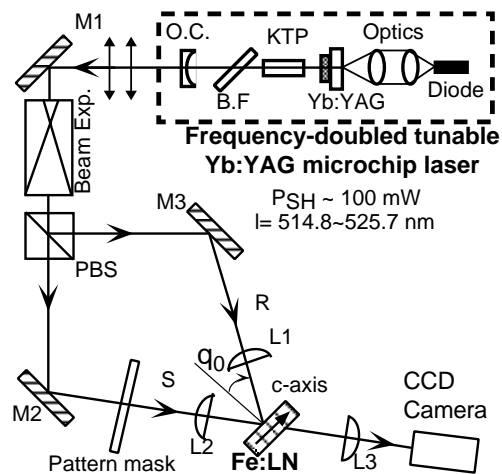


Figure 1. Holographic recording system by using intracavity frequency-doubled Yb:YAG microchip laser.

### VIII-D-2 Design Criteria for Optimization of Fiber-Coupled Diode Longitudinally-Pumped Laser Using Pump-beam $M^2$ Factor

PAVEL, Nicolaie<sup>1</sup>; KURIMURA, Sunao; TAIRA, Takunori

(<sup>1</sup>*Inst. Atm. Phys., Romania*)

For optimization of longitudinally-pumped solid-state lasers, a model which consider the pump-beam propagation described by its  $M^2$  factor is proposed. Analytical functions for the optimum focusing-position, the optimum pump spot-size, the minimum threshold pump power and the maximum overlap efficiency are given. A simple output to input power relation and previous formula provides a straightforward procedure to design the optimum laser resonator, the coupling-optics and to evaluate the laser output power.

A slope efficiency of 57% with a 53% optical-efficiency at maximum 8-W pump-power was obtained from a fiber-coupled longitudinally-pumped Nd:YAG medium. A very good agreement between experiments and theory was obtained.

#### References

- 1) R. A. Fields *et al.*, *Appl. Phys. Lett.* **51**, 1885 (1987).
- 2) T. Taira *et al.*, *Opt. Lett.* **16**, 1955 (1991).
- 3) M. D. Selker *et al.*, *CLEO CPD21*, (1996).
- 4) T. Taira *et al.*, *OSA TOPS* **19**, 430 (1998).

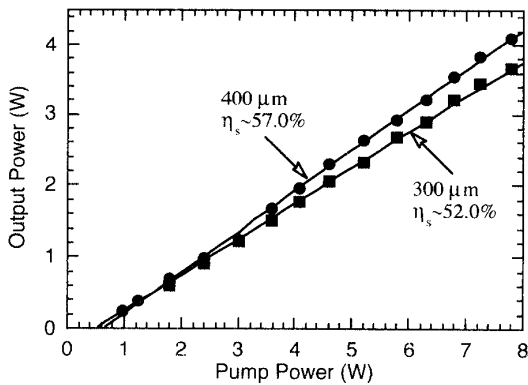


Figure 1. Output power as a function of pump-power.

### VIII-D-3 Highly Nd<sup>3+</sup>-Doped YAG Ceramic for Microchip Lasers

TAIRA, Takunori; KURIMURA, Sunao; SAIKAWA, Jiro; IKESUE, Akio<sup>1</sup>; YOSHIDA, Kunio<sup>2</sup>  
(<sup>1</sup>JFCC; <sup>2</sup>Osaka Inst. Tech.)

Nd:YVO<sub>4</sub> offers highly efficiency miniature or microchip lasers due to its high absorption and emission cross-sections.<sup>1-4</sup> However, its poor thermo-mechanical properties prevent high power laser operation. Much effort has gone into laser material research to find a high absorption coefficient laser medium with high thermal shock parameters. Lately, a high optical quality Nd:YAG laser material of polycrystalline ceramic has been reported.<sup>5</sup> In this paper, we have demonstrated a highly efficient oscillation in a Nd:YAG ceramic microchip laser.

The YAG ceramic allows highly neodymium-ion doping to overcome low absorption cross-section. The absorption coefficient of the single Nd:YAG crystal was 3.45 cm<sup>-1</sup> at 808 nm, while the 9.1 at.% Nd:YAG ceramic has about 10 times higher absorption. The absorption coefficient of the 4.8 at.% Nd:YAG ceramic was 11.7 cm<sup>-1</sup>. This result indicates that Nd:YAG ceramic has advantages in a microchip or miniature laser system as well as Nd:YVO<sub>4</sub>. The thermal conductivity of Nd:YAG ceramic decreases with Nd concentration and thermal conductivity of the 9.1 at.% doped YAG ceramic was 9.0 W/mK.

The 4.8 at.% Nd<sup>3+</sup> doped YAG ceramic was cut to a 847 μm thickness for microchip laser experiments. The plan-concave resonator configuration has an output mirror radius of 100-mm and a resonator length of 50-mm. The 808 nm pump beam was focused to a diameter of 100 μm in the medium. Figure 1 shows an output power of Nd:YAG ceramic laser as a function of input power. A performance of 0.9 at.% Nd:YAG single crystal also plotted in order to compare. As a result, the maximum output power of Nd:YAG ceramic laser was four times higher than conventional Nd:YAG single crystal laser because the YAG ceramic has over five times higher Nd<sup>3+</sup> ion doping level. Conventional ceramic laser has highly scattering loss which prevent the highly efficient laser oscillation. We are estimating an internal loss of laser cavity from the slope efficiency.

In summary, we developed highly Nd-doped YAG in ceramic for high power microchip laser. Four times higher laser output power in YAG ceramic compared

with conventional YAG single crystal was demonstrated.

### References

- 1) R. A. Fields *et al.*, *Appl. Phys. Lett.* **51**, 1885 (1987).
- 2) T. Taira *et al.*, *Opt. Lett.* **16**, 1955 (1991).
- 3) W. L. Nighan *et al.*, *Conf. Lasers and Electro-Optics*, OSA Tech. Dig.; Washington DC., paper CMD5 (1995).
- 4) M. D. Selker *et al.*, *Conf. Lasers and Electro-Optics*, OSA Tech. Dig.; Washington DC., paper CPD21 (1996).
- 5) T. Taira *et al.*, *TOPS* **19**, 430 (1998).

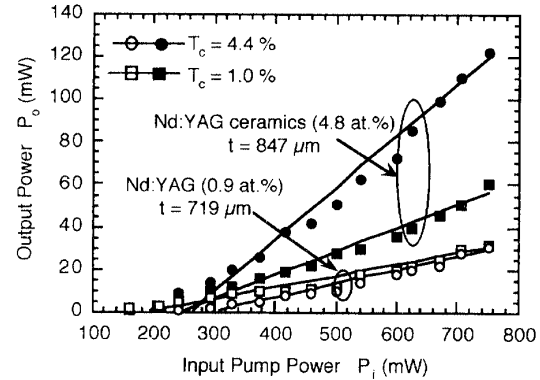


Figure 1. Input-output power characteristics of a diode-pumped Nd:YAG ceramic laser.

### VIII-D-4 Nondestructive Characterization of Quasi-Phase-Matched Wavelength Converter

KURIMURA, Sunao; UESU, Yoshiaki<sup>1</sup>  
(<sup>1</sup>Waseda Univ.)

We devised an observation technique of 180° domains in ferroelectric crystals by using Second Harmonic Generation (SHG) Microscope. The phase reversal of the SH wave accompanying inversion of spontaneous polarization is exploited to visualize domains. Interference between SH waves converts the phase information to the SH contrast. Domain mapping is achieved in LiNbO<sub>3</sub> and LiTaO<sub>3</sub> with nonlinear coefficients  $d_{33}$  and  $d_{22}$  under the microscope, which enables characterization of a periodically-poled structure in quasi-phase-matched wavelength converters in a nondestructive way. The validity of the technique is proved by another characterizing tool of destructive etching.

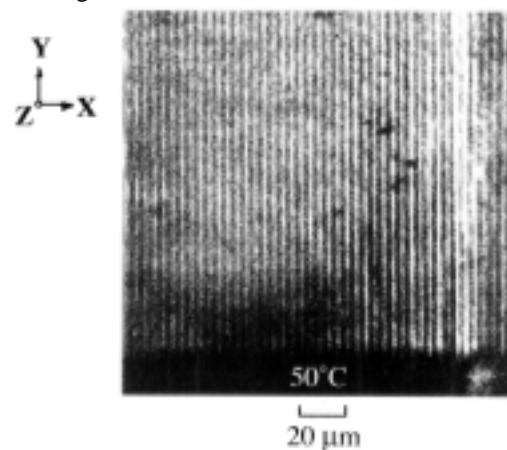


Figure 1. Photo of a Z-cut QPMLT device.

## Research Center for Molecular Materials

### VIII-E Development of Novel Heterocyclic Compounds and their Molecular Assemblies for Advanced Materials

Heterocycles containing sulfur and/or nitrogen atoms are useful as components of functional materials since heteroatoms in their rings are helpful to stabilize ions or ion-radical species, and extended  $\pi$ -conjugation decreases Coulombic repulsion. In addition intermolecular interactions caused by heteroatom contacts can be expected to form novel molecular assemblies. In this project new electron acceptors, donors, and donor-acceptor compounds based on heterocycles such as 1,2,5-thiadiazole and 1,3-dithiole were synthesized and their properties including those of the charge-transfer complexes or ion-radical salts were investigated. Unique crystal structures were constructed by using weak intermolecular interactions such as hydrogen bonding or heteroatom contacts. Thiophene oligomers with rigid structures were also synthesized for molecular wires.

#### VIII-E-1 Cation Radical Salts of TTF Vinylogues with $\text{Au}(\text{CN})_2$ Anion

YAMASHITA, Yoshiro; TOMURA, Masaaki; IMAEDA, Kenichi

TTF vinylogues bearing substituents have been easily obtained and the TTF skeletons can be planar when the aryl substituents are twisted from the  $\pi$ -conjugated framework. We have now found that TTF vinylogues **1a-c** containing one halogen atom at the ortho position afford cation radical salts  $[\mathbf{1}\cdot\text{Au}(\text{CN})_2]$  as single crystals when they are electrochemically oxidized in dichloromethane in the presence of  $\text{Bu}_4\text{N}\cdot\text{Au}(\text{CN})_2$ . The X-ray crystal structure analyses of  $\mathbf{1b,c}\cdot\text{Au}(\text{CN})_2$  salts were carried out to reveal the unique crystal structures. The molecular and crystal structure of  $\mathbf{1b}\cdot\text{Au}(\text{CN})_2$  is shown in Figure 1. The TTF vinylogue skeleton is planar and the phenyl groups are orthogonal from the  $\pi$ -framework. The donor molecules do not take a stacking structure and the 1,3-dithiole parts sandwich the counter anion. The crystal structure of  $\mathbf{1c}\cdot\text{Au}(\text{CN})_2$  is very similar to that of  $\mathbf{1b}\cdot\text{Au}(\text{CN})_2$ . These cation radical salts showed semiconducting behaviour since these have a 1:1 stoichiometry  $[\mathbf{1b}\cdot\text{Au}(\text{CN})_2]$ ;  $\sigma = 1 \times 10^{-2} \text{ Scm}^{-1}$ ,  $E_a = 0.11 \text{ eV}$ ,  $\mathbf{1c}\cdot\text{Au}(\text{CN})_2$ ;  $\sigma = 5 \times 10^{-3} \text{ Scm}^{-1}$ ,  $E_a = 0.11 \text{ eV}$ ].

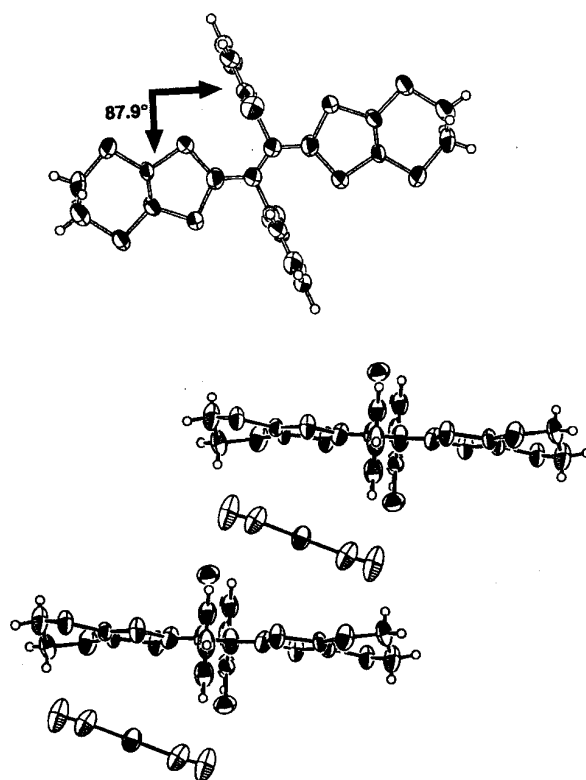
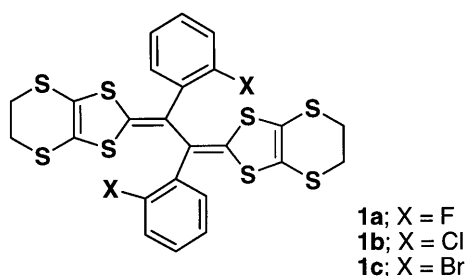


Figure 1. Molecular and crystal structure of  $\mathbf{1b}\cdot\text{Au}(\text{CN})_2$ .

#### VIII-E-2 Control of Packing Mode in Crystals of Cation Radical Salts of TTF Vinylogues

TOMURA, Masaaki; YAMASHITA, Yoshiro

Molecular and crystal structures of cation radical salts of novel tetrathiafulvalene (TTF) vinylogues with extended  $\pi$ -conjugation and aryl groups in their vinyl part have been studied by X-ray crystallographic analysis. We reported that the unique conformation with a planar TTF vinylogue framework in  $\mathbf{1}\cdot\text{PF}_6$  salt causes an interesting two-dimensional stacking mode where one donor molecule bridges two molecules like a brick wall in the crystal.<sup>1)</sup> We have succeeded in controlling the packing mode in the two-dimensional stack by changing the counter anion. In the case of  $\mathbf{1}\cdot\text{FeCl}_4$  salt, we observed a partial two-dimensional stacking in the crystal. On the other hand, the zigzag two-dimensional

stacking with an angle of nearly 90° exists in the crystal of **1**-ReO<sub>4</sub> salt, as shown in Figure 1.

#### Reference

- 1) Y. Yamashita, M. Tomura, M. B. Zaman and K. Imaeda, *Chem. Commun.* 1657 (1998).

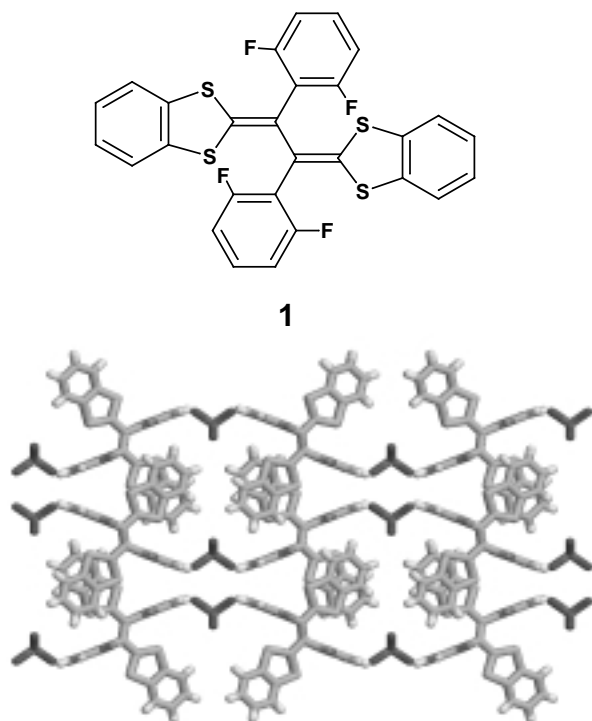


Figure 1. Crystal structure of **1**-ReO<sub>4</sub> salt.

#### VIII-E-3 Non-Planar BEDT-TTF Derivatives Fused with Tetrahydrofuran Rings Affording Cation Radical Salts with Unusual Structures

YAMASHITA, Yoshiro; TOMURA, Masaaki

Unusual crystal structures are expected from non-planar molecules to avoid steric interactions. Three-component conductors might be prepared from non-planar molecules by inclusion of solvent molecules. We have now designed new electron donors **1** and **2** where tetrahydrofuran (THF) rings are fused to BEDT-TTF. The new donors were prepared using the addition reaction of oligo(1,3-dithiole-2,4,5-trithione) with 2,5-dihydrofuran. The donor **2** gave two cation radical salts [**2**·Au(CN)<sub>2</sub> and **2**·PF<sub>6</sub>·(PhCl)<sub>0.5</sub>] as single crystals when electrochemically oxidized in chlorobenzene. The salts exhibit semiconducting behavior [**2**·Au(CN)<sub>2</sub>;  $\sigma = 3 \times 10^{-3} \text{ Scm}^{-1}$ ,  $E_a = 0.20$ , **2**·PF<sub>6</sub>·(PhCl)<sub>0.5</sub>;  $\sigma = 5 \times 10^{-5} \text{ Scm}^{-1}$ ,  $E_a = 0.24 \text{ eV}$ ]. The X-ray crystal analyses of these salts revealed their unusual crystal structures. The donor molecule is non-planar and the cis-fused THF ring is like a hook. In **2**·Au(CN)<sub>2</sub> one Au(CN)<sub>2</sub> anion is sandwiched between the donor molecules. This sandwiched structure is stacked to give a column. In **2**·PF<sub>6</sub>·(PhCl)<sub>0.5</sub>, instead of a stacking structure, a complicated molecular network is observed, where one neighboring molecule is highly leaned (77°) and the molecules are combined by short S...S contacts as

shown in Figure 1.

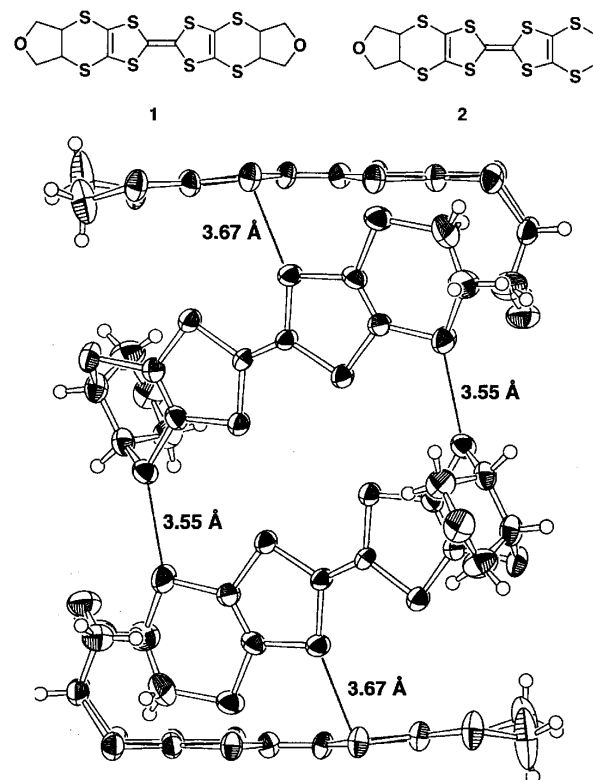


Figure 1. Crystal structure of **2**·PF<sub>6</sub>·(PhCl)<sub>0.5</sub>.

#### VIII-E-4 Bithiophene-TCNQ Analogue with Fused 1,2,5-Thiadiazole Rings

SUZUKI, Kazuharu; TOMURA, Masaaki; YAMASHITA, Yoshiro

Sulfur containing TCNQ analogues are highly polarized and are expected to have strong intermolecular interactions by heteroatom contacts. We have now prepared  $\pi$ -extended electron acceptor **1** containing fused thiadiazole rings and carried out the X-ray structure analysis to reveal the intermolecular interactions. The acceptor **1** was obtained by the reaction of dibromide **2** with tetracyanoethylene oxide (TCNEO) in 3% yield. However, thiophen-TCNQ analogue **3** could not be isolated in this reaction. The mechanism for the formation of **1** is still ambiguous. In the reaction to give **1**, a small amount of new compound **4** was isolated whose structure was determined by X-ray structure analysis. The dibromide **4** gave **1** upon heating, suggesting that **4** is an intermediate to give **1**. The absorption maximum of **1** is observed at 461 nm in dichloromethane. The reduction potential (-0.31 V vs. SCE) is lower than that of TCNQ, indicating that the interaction between the dicyanomethylene parts is weak in **1**. The X-ray analysis revealed that **1** forms a molecular assembly by heteroatom interactions. The crystal structure is shown in Figure 1. The planar molecules are combined by short S...N contacts to give a three-dimensional network. The distance of S...N contact (3.18 Å) is shorter than the sum of the van der Waals distances (3.35 Å).

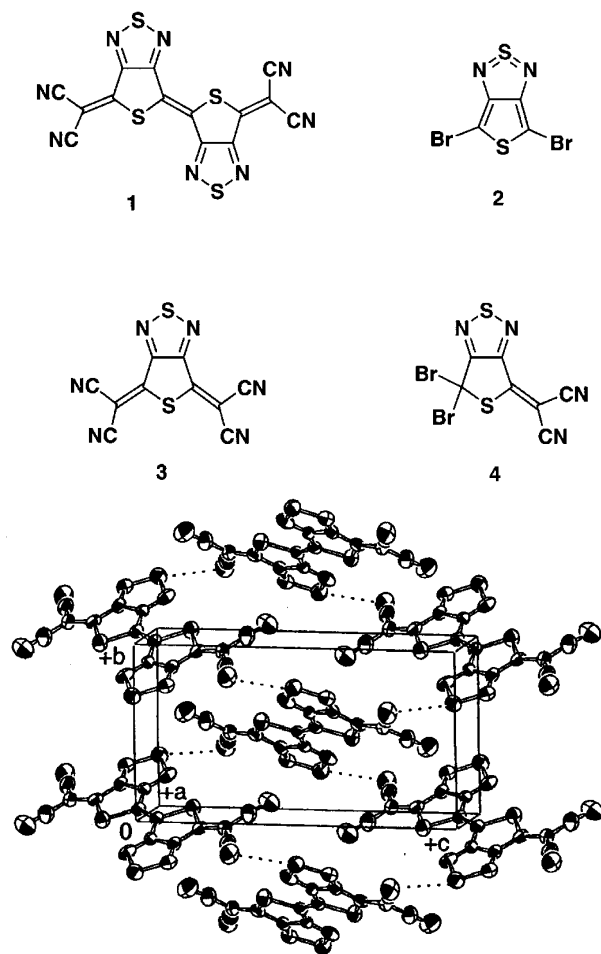


Figure 1. Crystal structure of **1**.

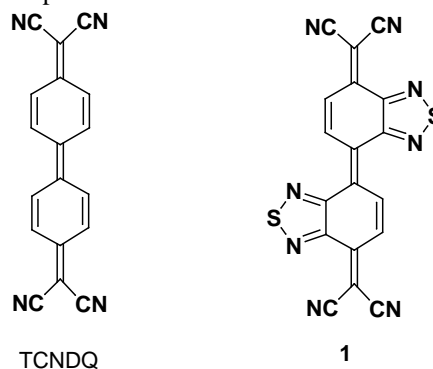
#### VIII-E-5 First Stable Tetracyanodiphenoquinodimethane with a Completely Planar Geometry: Preparation, X-Ray Structure, and Highly Conductive Complexes of Bis[1,2,5]thiadiazolo-TCNDQ

FUKUSHIMA, Takanori<sup>1</sup>; OKAZERI, Nobuharu<sup>1</sup>; MIYASHI, Tsutomu<sup>1</sup>; SUZUKI, Kazuharu; YAMASHITA, Yoshiro; SUZUKI, Takanori<sup>2</sup>  
(<sup>1</sup>Tohoku Univ.; <sup>2</sup>Hokkaido Univ.)

[*Tetrahedron Lett.* **40**, 1175 (1999)]

The title tetracyanodiphenoquinodimethane (TCNDQ) derivative **1** was newly designed and prepared as a novel component for highly conductive organic materials. This is the first stable TCNDQ derivative which is a  $\pi$ -extended electron acceptor. The synthesis was achieved by using Pd(0)-catalyzed reaction of the corresponding diiodo compound with NaCH(CN)<sub>2</sub> followed by oxidation. Introduction of thiadiazole rings into the TCNDQ skeleton leads to large stabilization in the neutral state. X-ray analysis has revealed the unique structure, where interatomic interactions (CH $\cdots$ N, S $\cdots$ N) play an important role in determining the molecular and crystal structure. The novel electron acceptor shows strong electron affinity ( $E_{\text{red}} = +0.33, +0.12$  V vs. SCE in CH<sub>2</sub>Cl<sub>2</sub>) comparable with that of TCNQ, and gave highly conductive charge

transfer complexes and anion radical salts.



#### VIII-E-6 Novel Supramolecular Synthons in Crystal Engineering: Ionic Complexes of 4,4'-Bipyridine and 1,2-Bis(2-pyridyl)ethylene with 2,5-Dichloro-3,6-dihydroxy-1,4-benzoquinone

ZAMAN, Md. Badruz; TOMURA, Masaaki; YAMASHITA, Yoshiro

[*Chem. Commun.* 999 (1999)]

In order to develop a new type of hydrogen-bonding system, we have selected bipyridine (BPY) and 1,2-bis(2-pyridylethylene) (2-PDE) as proton acceptor, and chloranilic acid (2H-CLA) as proton donor. The complexes were prepared by reacting BPY and 2-PDE with an equal amount of 2H-CLA in acetone and/or a mixture of acetone-MeOH. The crystal structure analysis revealed that molecular complexes [BPY-2H]<sup>2+</sup>[CLA]<sup>2-</sup> **1** and [2-PDE-2H]<sup>2+</sup>[CLA]<sup>2-</sup> **2** are formed where proton transfer occurs. The component molecules are combined via three-center hydrogen bonded interactions to build a linear molecular chain for **1** and a zigzag molecular tape for **2**. The structure of **1** is shown in Figure 1. In both **1** and **2**, bifurcated interionic [N<sup>+</sup>-H $\cdots$ O<sup>-</sup> and N<sup>+</sup>-H $\cdots$ O] hydrogen bonds between the nitrogen atoms of the cations and the two oxygen atoms from the anions are observed. This is a new supramolecular synthon motif. In complex **1** alternating DA-type pairs of the cation and anion molecules are observed in the stacking, while complex **2** has a segregated stacking assembly as DD- and AA-type pairs.

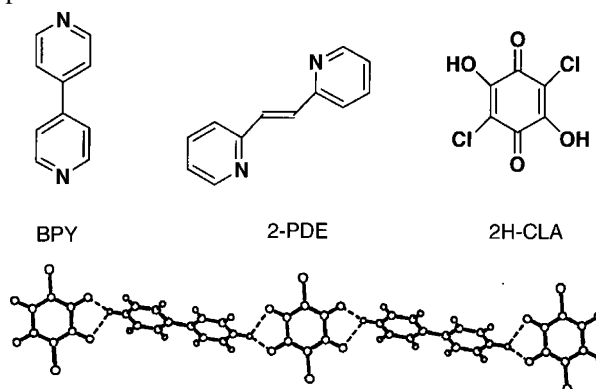


Figure 1. Hydrogen bonding in **1**.

### VIII-E-7 Design and Synthesis of Soluble Linear Macromolecules with Highly Extended $\pi$ -Conjugated Backbone

TANAKA, Shoji; YAMASHITA, Yoshiro

The development of soluble linear macromolecules with highly extended  $\pi$ -conjugated system is of crucial importance to establish the structure-conductance relationship in ballistic-type molecular electric wires. Although the introduction of alkyl substituents into the main chain is an effective method to improve the solubility, this modification often results in conjugation defects in the main chain due to the enhanced inter-unit steric repulsion. Here we report on a tactics in molecular design to do well both in solubility and  $\pi$ -conjugation of

linear oligomers. We have synthesized a series of mixed oligomers **1-5**. All of the alkyl-substituted oligomers are more soluble in  $\text{CH}_2\text{Cl}_2$ ,  $\text{CHCl}_3$ , and THF compared with the unsubstituted ones. As shown in Figure 1, the hexyl substitution on **1a** induces only a small blue shift of the absorption maximum, indicating a tiny loss of conjugation in spite of the long alkyl-chain substitution. These results suggest that **1b** unit can be used as a building block for soluble and effectively  $\pi$ -conjugated macromolecules. Along this line, we have obtained soluble highly oligomers **1c-d**. The red shift values induced by the chain extension (**1b**  $\rightarrow$  **1c**  $\rightarrow$  **1d**) are significantly higher than the shift value of the related oligomers (**3c**  $\rightarrow$  **3d**). This supports the highly extended  $\pi$ -conjugation in the main chain of **1c-d**.

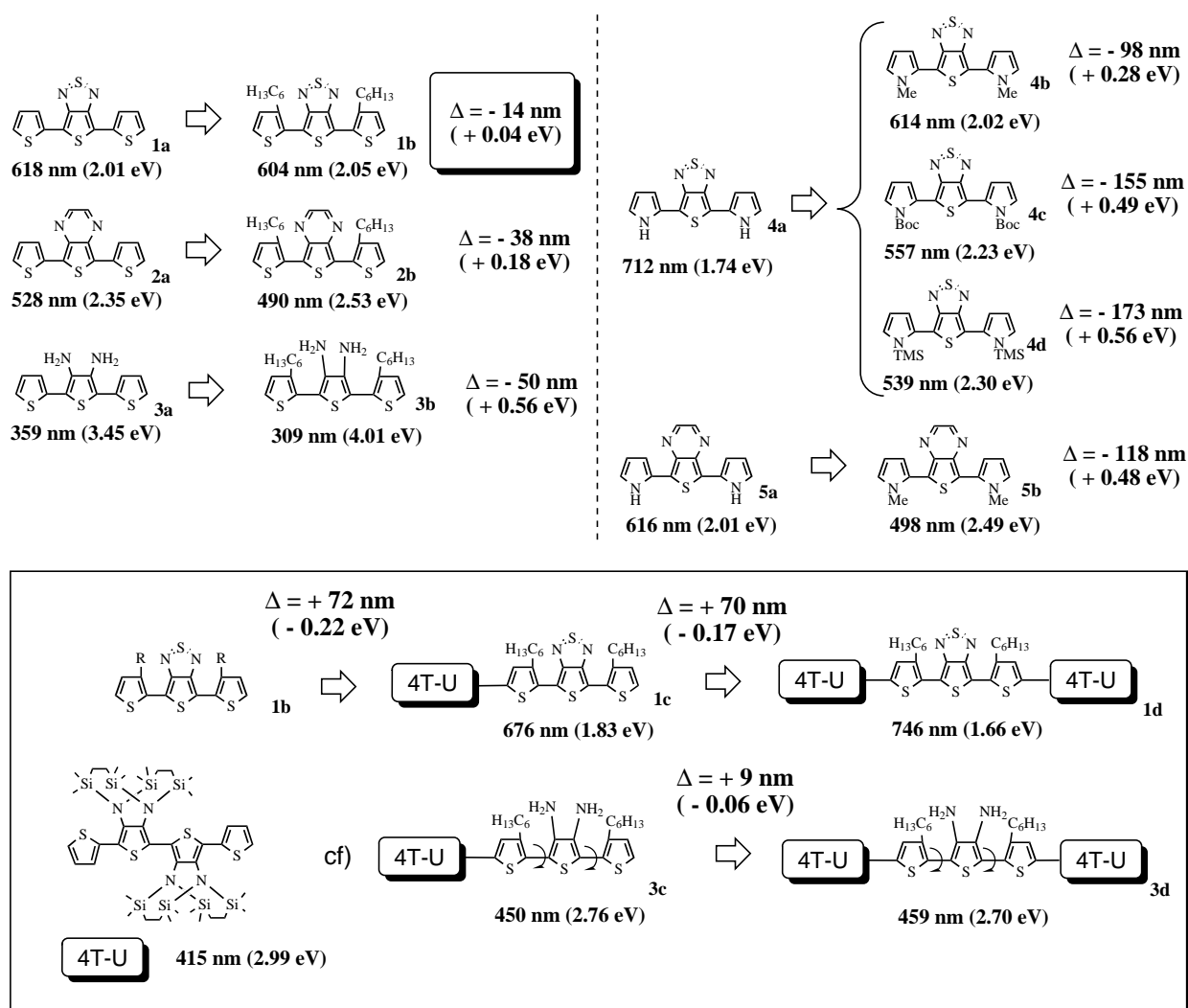


Figure 1. Substituent effects on the absorption maximum of the obtained mixed oligomers.

## VIII-F Electronic Structures and Reactivities of Active Sites of Metalloproteins

Metalloproteins are a class of biologically important macromolecules which have various functions such as oxygen transport, electron transfer, oxidation, and oxygenation. These diverse functions of metalloproteins have been thought to depend on the ligands from amino acid, coordination structures, and protein structures in immediate vicinity of metal ions. In this project, we are studying the relationship between the structures of the metal active sites and functions of metalloproteins.

### VIII-F-1 High-Spin (*meso*-Tetraalkylporphyrinato)iron(III) Complexes As Studied by X-ray Crystallography, EPR, and Dynamic NMR Spectroscopies

IKEUE, Takahisa<sup>1</sup>; OHGO, Yoshiki<sup>1</sup>; UCHIDA, Akira<sup>1</sup>; NAKAMURA, Mikio<sup>1</sup>; FUJII, Hiroshi; YOKOYAMA, Masataka<sup>2</sup>  
(<sup>1</sup>Toho Univ.; <sup>2</sup>Chiba Univ.)

[*Inorg. Chem.* **38**, 1276 (1999)]

<sup>1</sup>H-NMR spectra of a series of high-spin (*meso*-tetraalkylporphyrinato)iron(III) chlorides, [Fe(TRP)Cl] where R = Me, Et, Pr, or iPr, have been measured at various temperatures in CD<sub>2</sub>Cl<sub>2</sub> solution. In the case of the Et, Pr, and iPr complexes, either the methyl or the methylene signal split into two signals with equal integral intensities at low temperature. In contrast, the Me complex did not show any splitting even at -100 °C. The results have been ascribed to the hindered rotation of the *meso*-alkyl groups about C<sub>meso</sub>-C bonds. The activation free energies for rotation have been determined as 8.0 (-72 °C), 8.5 (-60 °C), and 8.9 (-62 °C) kcal·mol<sup>-1</sup> for the Et, Pr, and iPr complexes, respectively, at coalescence temperatures given in parentheses. The small activation free energy for rotation of the isopropyl groups observed in the present system is explained in terms of the nonplanarity of the porphyrin ring, which has been verified both by the X-ray crystallographic analysis and by the EPR spectrum taken in a frozen CH<sub>2</sub>Cl<sub>2</sub>-toluene solution. The success in observing the hindered rotation of less bulky primary alkyl groups such as ethyl and propyl groups at an easily accessible temperature range is attributed to the large difference in chemical shifts of the mutually exchanging protons, *ca.* 3500 Hz in the case of the Et complex, caused by the paramagnetism of the five-coordinated ferric porphyrin complexes.

### VIII-F-2 Insensitivity of Vanadyl-Oxygen Bond Strengths to Radical Type (<sup>2</sup>A<sub>1u</sub> vs. <sup>2</sup>A<sub>2u</sub>) in Vanadyl Porphyrin Cation Radicals

CZARNECKI, Kazimierz<sup>1</sup>; PRONIEWICZ, Leonard M.<sup>1</sup>; FUJII, Hiroshi; JI, David<sup>2</sup>; CZERNUSZEWICZ, Roman S.<sup>2</sup>; KINCAID, James R.<sup>1</sup>  
(<sup>1</sup>Marquette Univ.; <sup>2</sup>Univ. Houston)

[*Inorg. Chem.* **38**, 1543 (1999)]

Resonance Raman (RR) spectra are reported for vanadyl octaethylporphyrin, O=V(OEP), tetramesityl-tetramethylporphyrin, O=V(TMTMP), and tetramesityl-

porphyrin, O=V(TMP), and their corresponding  $\pi$ -cation radicals obtained by chemical and electrochemical oxidation. The behavior of the  $\nu_2$  RR porphyrin "marker band," which moves to higher frequency upon oxidation of the O=V(OEP) and O=V(TMTMP) and to lower frequency for O=V(TMP), shows that the resultant cation radicals have predominantly <sup>2</sup>A<sub>1u</sub> and <sup>2</sup>A<sub>2u</sub> ground states, respectively. In contrast to earlier work (K. A. Macor, R. S. Czernuszewicz and T. G. Spiro, *Inorg. Chem.* **29**, 1990 (1996)), it is demonstrated here that the shift of the  $\nu(V=O)$  is insensitive to radical type, behavior which is in agreement with similar studies of the ferryl analogues (K. Czarnecki *et al.*, *J. Am. Chem. Soc.* **116**, 2929 and 4680 (1996)). It is suggested that the observed downshifts of the  $\nu(V=O)$  previously reported for RR spectra of vanadyl porphyrin  $\pi$ -cation radicals, relative to their neutral parents, are most reasonably ascribed to trans oxo ligand coordination (most probably a water molecule) during low-temperature electrochemical oxidation of the neutral species.

### VIII-F-3 Electron Configuration of Ferric Ions in Low-Spin (Dicyano)(*meso*-tetraarylporphyrinato)iron(III) Complexes

NAKAMURA, Mikio<sup>1</sup>; IKEUE, Takahisa<sup>1</sup>; IKEZAKI, Akira<sup>1</sup>; OHGO, Yoshiki<sup>1</sup>; FUJII, Hiroshi  
(<sup>1</sup>Toho Univ.)

[*Inorg. Chem.* **38**, 3857 (1999)]

The electron configuration of a series of low-spin (dicyano){*meso*-tetrakis(2,4,6-trialkylphenyl)porphyrinato}iron(III) complexes, [Fe(R-TPP)(CN)<sub>2</sub>]<sup>-</sup> where R = Me, Et, or iPr, together with the parent [Fe(TPP)(CN)<sub>2</sub>]<sup>-</sup>, has been examined in dichloromethane-methanol solution by <sup>1</sup>H-NMR, <sup>13</sup>C-NMR, and EPR spectroscopies. While the ferric ion of [Fe(TPP)(CN)<sub>2</sub>]<sup>-</sup> has shown a common (d<sub>xy</sub>)<sup>2</sup>(d<sub>xz</sub>,d<sub>yz</sub>)<sup>3</sup> configuration, the ferric ions of the alkyl-substituted complexes [Fe(R-TPP)(CN)<sub>2</sub>]<sup>-</sup> have exhibited the preference of a less common (d<sub>xz</sub>,d<sub>yz</sub>)<sup>4</sup>(d<sub>xy</sub>)<sup>1</sup> configuration. Spectroscopic characteristics of the complexes in which ferric ions take the (d<sub>xz</sub>,d<sub>yz</sub>)<sup>4</sup>(d<sub>xy</sub>)<sup>1</sup> configuration are (i) axial type EPR spectra, (ii) downfield shifted pyrrole and meta signals in <sup>1</sup>H-NMR spectra, and (iii) downfield shifted *meso*-carbon signals in <sup>13</sup>C-NMR spectra. Occurrence of the less common (d<sub>xz</sub>,d<sub>yz</sub>)<sup>4</sup>(d<sub>xy</sub>)<sup>1</sup> configuration in [Fe(R-TPP)(CN)<sub>2</sub>]<sup>-</sup> has been ascribed to the electronic interaction between iron(d) and cyanide(p\*) orbitals. The interaction stabilizes the d orbitals and induces (d<sub>xz</sub>,d<sub>yz</sub>)<sup>4</sup>(d<sub>xy</sub>)<sup>1</sup> configuration. Since the electron configuration of (dicyano){*meso*-tetrakis(2,6-dichloro-

phenyl)porphyrinato}iron(III),  $[\text{Fe}(\text{Cl-TPP})(\text{CN})_2]^-$ , which carries bulky electronegative chlorine atoms at the ortho positions, is presented as a common  $(d_{xy})^2(d_{xz}, d_{yz})^3$ , the less common  $(d_{xz}, d_{yz})^4(d_{xy})^1$  configuration in  $[\text{Fe}(\text{R-TPP})(\text{CN})_2]^-$  can be ascribed, at least partially, to the electron-donating ability of the meso-aryl groups.

#### VIII-F-4 Resonance Raman Spectra of Legitimate Models for the Ubiquitous Compound I Intermediates of Oxidative heme Enzymes

**CZARNECKI, Kazimierz<sup>1</sup>; KINCAID, James R.<sup>1</sup>; FUJII, Hiroshi**  
(<sup>1</sup>Marquette Univ.)

[*J. Am. Chem. Soc.* in press]

Resonance Raman (RR) spectra are reported for two models of the compound I intermediates of oxidative heme proteins; namely, the imidazole (Im) and 2-methyl-imidazole (2-MeIm) complexes of the ferryl  $\pi$ -cation radical derivative of iron-(5,10,15,20-tetramesitylporphyrin),  $[\text{O}=\text{Fe}(\text{TMP}^{+\bullet})(\text{Im})]^+$  and  $[\text{O}=\text{Fe}(\text{TMP}^{+\bullet})(2\text{-MeIm})]^+$ , which are stabilized in dichloromethane solution at  $-80^\circ\text{C}$ . The present study yields high quality RR spectra of these complexes and provides the first opportunity to compare the  $\nu(\text{Fe}=\text{O})$  stretching modes and the structure-sensitive core marker modes for a ferrylporphyrin  $\pi$ -cation radical with the corresponding modes of the neutral parent bearing the same trans-axial ligand. While the observed shifts in the frequencies of the core modes are in agreement with those expected upon formation of the  $\pi$ -cation radical, the results suggest that the isolated effect of macrocycle oxidation on the  $\text{Fe}=\text{O}$  stretching frequency is rather small; the observed shift being only about  $4\text{ cm}^{-1}$  to lower frequency.

#### VIII-F-5 Newly Designed Iron-Schiff Base Complexes as Models of Mononuclear Non-Heme Iron Active Sites

**FUNAHASHI, Yasuhiro; FUJII, Hiroshi**

High valent iron-oxo species have been suggested as the active intermediates for catalytic oxygenation

reactions by iron-containing oxygenases. In the reaction mechanisms of heme and binuclear non-heme iron enzymes, an  $\text{Fe}^{\text{IV}}=\text{O}$  porphyrin radical species (Compound I) and a  $\text{Fe}^{\text{IV}}_2(\mu\text{-O})_2$  species (Intermediate Q) have been found to be responsible oxidant for alkane hydroxylation and alkene epoxidation. Such the high valent iron-oxo species are inferred to involve in hydroxylation of aromatic compounds by mononuclear non-heme iron oxygenases, the reaction processes of which, however, still remains to be established. In order to gain insight into the active intermediates, we try to synthesize iron complexes with bulky schiff-base ligands as biomimetic models of mononuclear non-heme iron active sites. The active oxygen adduct of these complexes, which would be kinetically stabilized by their steric hindrance, might provide a basis for understanding the oxygenation by mononuclear iron sites.

#### VIII-F-6 <sup>17</sup>O-NMR Study of Oxygen Molecules Bound to Copper Ions of Mononuclear and Dinuclear Copper Complexes

**MIZUTANI, Mamoru; FUJII, Hiroshi**

The activation of molecular oxygen by transition metals has fascinated chemists for decades. In particular copper-dioxygen complexes are suggested as key reaction intermediates in many enzymatic reactions. The differentiation in the function of these copper enzymes is attributed primarily to the coordination structure of the copper-dioxygen intermediate formed in the protein matrices, depending on the ligand donors, the geometry, and the coordination mode of the dioxygen. However, the correlation between these structural factors and the function/catalysis of the enzymes remains to be elucidated. To this end, there have been reported the structural and/or functional model complexes of copper-dioxygen adducts, such as  $\mu$ -peroxo complex and  $\mu$ - $\eta_2, \eta_2$  complex. The copper-bound dioxygen is not activated when it is end-on structure but activated via O-O bond cleavage when it is side-on structure. In order to investigate the relationships between electronic structure and reactivity of copper-dioxygen complex, we have examined <sup>17</sup>O-NMR spectroscopies of several copper-dioxygen complexes.

## VIII-G Molecular Mechanism of Heme Degradation and Oxygen Activation by Heme Oxygenase

Heme oxygenase (HO), an amphipathic microsomal proteins, catalyzes the regiospecific oxidative degradation of iron protoporphyrin IX (heme) to biliverdinIX $\alpha$ , carbon monoxide, and iron in the presence of NADPH-cytochrome P-450 reductase, which functions as an electron donor. Heme oxygenase reaction is the biosynthesis processes of bile pigments and CO which is a possible physiological messenger. Recent development in the bacterial expression of a soluble form of heme oxygenase has made it possible to prepare in the large quantities for structural studies. In this project, we are studying the molecular mechanism of heme degradation and the oxygen activation by heme oxygenase using various spectroscopic methods.

### VIII-G-1 Molecular Oxygen Oxidizes the Porphyrin Ring of the Ferric $\alpha$ -Hydroxyheme in Heme Oxygenase in the Absence of Reducing Equivalent

MIGITA, Catharina T.<sup>1</sup>; FUJII, Hiroshi; MATERA, Kathryn M.<sup>1</sup>; TAKAHASHI, Satoshi<sup>2</sup>; ZHOU, Hong<sup>3</sup>; YOSHIDA, Tadashi<sup>3</sup>; IKEDA-SAITO, Masao<sup>1</sup>  
 (<sup>1</sup>Case Western Reserve Univ.; <sup>2</sup>RIKEN; <sup>3</sup>Yamagata Univ.)

[*Biochim. Biophys. Acta* **1432**, 203 (1999)]

Heme oxygenase catalyzes the regiospecific oxidative degradation of iron protoporphyrin IX (heme) to biliverdin, CO and Fe, utilizing molecular oxygen and electrons donated from the NADPH-cytochrome P450 reductase. The catalytic conversion of heme proceeds through two known heme derivatives,  $\alpha$ -hydroxyheme and verdoheme. In order to assess the requirement of reduction equivalents, we have prepared the  $\alpha$ -hydroxyheme complex with rat heme oxygenase isoform-1 and examined its reactivity with molecular oxygen in the absence of added electrons. Upon reaction with oxygen, a minor portion of the  $\alpha$ -hydroxyheme in heme oxygenase is converted to verdoheme with the majority altered to a species which exhibits an optical absorption spectrum with a broad Soret band. The major species, which is EPR-silent, can be converted to the original  $\alpha$ -hydroxyheme by addition of sodium dithionite. We have also found that oxidation of the  $\alpha$ -hydroxyheme-heme oxygenase complex by ferricyanide or iridium chloride yields a species which exhibits an optical absorption spectrum and reactivity similar to those of the main product of the oxygen reaction. We infer that the oxygen reaction with the ferric  $\alpha$ -hydroxyheme-heme oxygenase complex forms a ferric-porphyrin cation radical. We conclude, inconsistent to a previous report (Y. Liu, P. Moenne-Loccoz, T. M. Loehr and P. R. Ortiz de Montellano, *J. Biol. Chem.* **272**, 6909 (1997)), that in the absence of reducing agents, the oxygen molecule functions mainly as an oxidant for the porphyrin ring and has no role in the oxygenation of  $\alpha$ -hydroxyheme. This result corroborates our previous conclusion that the catalytic conversion of  $\alpha$ -hydroxyheme to verdoheme by heme oxygenase requires one reducing equivalent along with molecular oxygen.

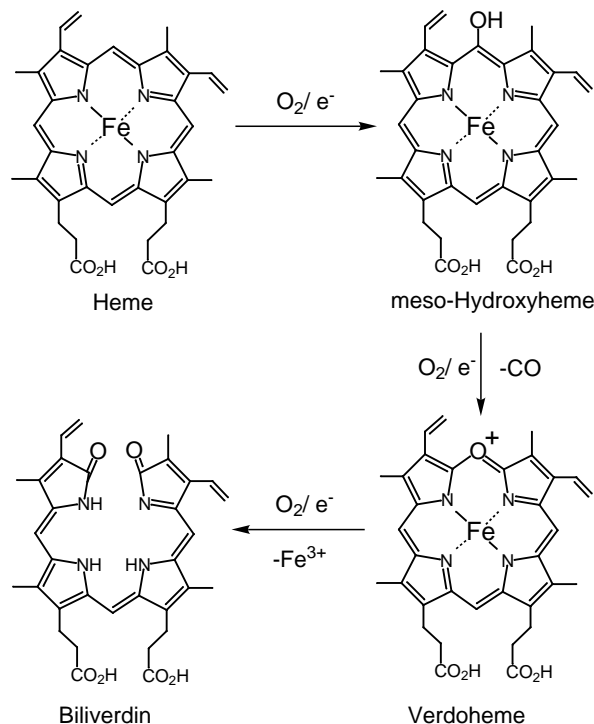


**Figure 1.** Reaction intermediates in the heme oxygenase catalyzed oxidation of heme to biliverdinIX $\alpha$ .

## VIII-H Designing Artificial Photosynthesis at Molecular Dimensions

Photosynthesis is one of the finest piece of molecular machinery that Nature has ever created. Its ultrafast electron transfer and following well-organized sequence of chemical transformation have been, and will continue to be, challenging goals for molecular scientists. We are trying to mimic the function of photosynthesis by assembling molecular units that perform individual physical/chemical action. The molecular units include porphyrins, redox active organic molecules, and transition metal complexes.

Our present efforts focus on chemistry of manganese complexes (which are known to play a key role in oxygenic photosynthesis), and photochemistry of porphyrin/transition metal complex dyads. Our ultimate goal is to design artificial molecular systems that effect multiple chemical reactions triggered by light, on the basis of molecular rationale.

### VIII-H-1 Synthesis and Characterization of Manganese Complexes

AIKAWA, Katsuji<sup>1</sup>; NAGATA, Toshi  
(<sup>1</sup>Kyoto Univ.)

In search for rationally designed dimanganese complexes that catalyze four-electron oxidation of water to dioxygen, we developed two xanthene-based dinucleating ligands, XT-btpa and XT-bterpy (Figure 1).

The XT-btpa (xanthene-bis(tris(2-pyridylmethyl)-amine) ligand has two metal-binding sites that are located in a well-defined geometry determined by the rigid xanthene spacer. The manganese complex was found to have an  $[\text{Mn}_2(\mu\text{-O})_2]$  core.

The XT-bterpy ligand also has two metal-binding sites with a well-defined geometry, and has two terpyridine units which provide more rigid and less decomposition-prone organic environment. Three manganese complexes,  $[(\text{XT-bterpy})\text{Mn}_2\text{Cl}_4]$ ,  $[(\text{XT-bterpy})\text{Mn}_2(\text{tropolonato})_2](\text{ClO}_4)_2$ , and  $[(\text{XT-bterpy})\text{Mn}_2(2\text{-picolinato})_2](\text{ClO}_4)_2$ , were prepared; the X-ray structure of  $[(\text{XT-bterpy})\text{Mn}_2\text{Cl}_4]$  is shown in Figure 2. Either of these three complexes catalyzed disproportionation of  $\text{H}_2\text{O}_2$  to water and dioxygen, with much higher activity than the related mononuclear complex  $[(\text{terpyridine})\text{MnCl}_2]$ .

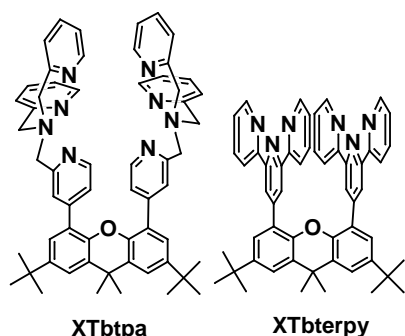


Figure 1. Two xanthene-based binucleating ligands.

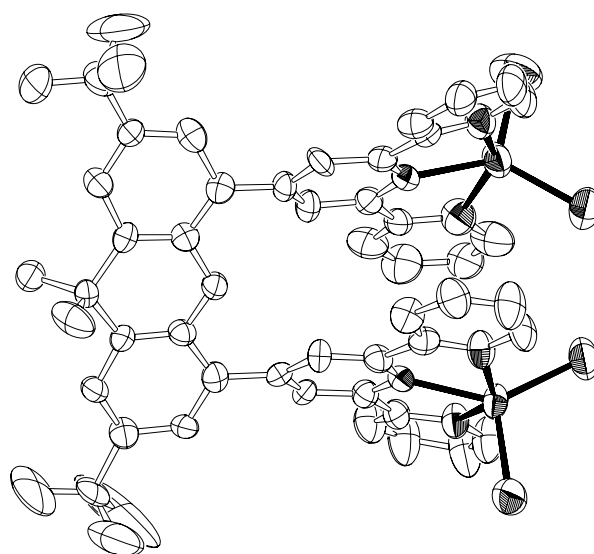


Figure 2. X-ray structure of  $[(\text{XT-bterpy})\text{Mn}_2\text{Cl}_4]$ .

### VIII-H-2 Synthesis and Photochemical Reaction of Porphyrin/Cobalt-complex Dyad Molecules

KIKUZAWA, Yoshihiro<sup>1</sup>; NAGATA, Toshi;  
OSUKA, Atsuhiko<sup>1</sup>  
(<sup>1</sup>Kyoto Univ.)

One of the essential features in natural photosynthetic reaction centers is ejection of the quinone acceptor from the protein to the "quinone pool," which takes place after photoinduced electron transfer. To mimic this function, we prepared a porphyrin/Co(III)-complex dyad molecule (Figure 1), where the Co(III) moiety is expected to depart from the porphyrin moiety after photoreduction, due to the relative instability of six-coordinate Co(II) complex. The steady-state fluorescence spectrum of this dyad molecule revealed that the excited singlet state of the porphyrin is effectively quenched by the presence of the Co(III) moiety. Electrochemical estimation of the reduction/oxidation potentials suggested photoinduced electron transfer from the excited porphyrin to Co(III) can take place. Irradiation of this dyad molecule in  $\text{CD}_3\text{COCD}_3/\text{CD}_3\text{-CN}$  solution led to formation of the Co(III)- $\text{CD}_3\text{CN}$  complex (80% yield by  $^1\text{H}$  NMR) together with the imidazolyl porphyrin without the cobalt moiety. Since this ligand-exchange reaction proceeds only slowly in the absence of light, it is likely that the reaction is

catalyzed by intramolecular photoinduced electron transfer.

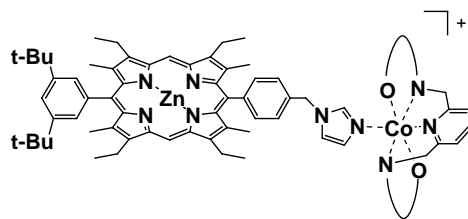


Figure 1. The porphyrin/cobalt(III)-complex dyad molecule.

## VIII-I Development of New Metal Complexes as Redox Catalysts

Redox catalysis is an important field of chemistry which translates a flow of electron into chemical transformation. It is also one of the requisites for artificial photosynthesis. This project of ours aims at developing new metal complexes that perform redox catalysis at low overpotential. So far we have succeeded in preparing a series of terpyridine-catechol linked ligands; application of these ligands for development of new redox catalysts is currently in progress.

### VIII-I-1 Synthesis of Terpyridine-catechol Linked Ligands and Their Cobalt(III) Complexes

NAGATA, Toshi; TANAKA, Koji

Transition metal catechol complexes are gaining interest because of unique electronic properties of the catechol ligand, specifically the two-electron redox transformation between catechol and quinone forms. Combination with the terpyridine ligand should provide metal complexes with interesting redox properties and well-defined geometry. The chemistry of terpyridine/catechol/metal ternary complexes, however, is often complicated by ligand disproportionation to give stable bis(terpyridine) complexes.

We prepared three terpyridine-catechol linked ligands (Figure 1) and their cobalt(III) complexes. The X-ray structure of two Co(III) complexes are shown in Figure 2. The two complexes have a different number of CH<sub>2</sub> units in the linker between terpyridine and catechol. It was revealed that the C<sub>4</sub> linked complex (part a) has a symmetric structure with the (CH<sub>2</sub>)<sub>4</sub> linker running along an approximate mirror plane that contains the catechol ring and bisects the terpyridine ligand, whereas the C<sub>5</sub> linked complex (part b) has no such approximate symmetry. Since the local structures around the Co(III) center are very similar for the two complexes, the structural difference is solely due to the different lengths of the polymethylene linkers; the C<sub>4</sub> linker presents the "just fit" length while the C<sub>5</sub> linker has to go the winding way to accommodate the extra CH<sub>2</sub> unit.

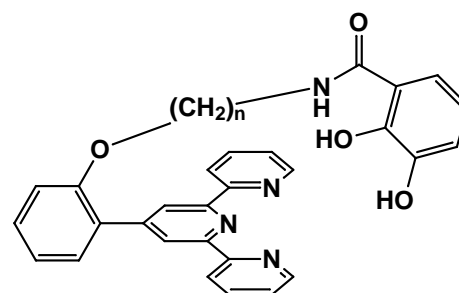


Figure 1. The terpyridine-catechol linked ligands.

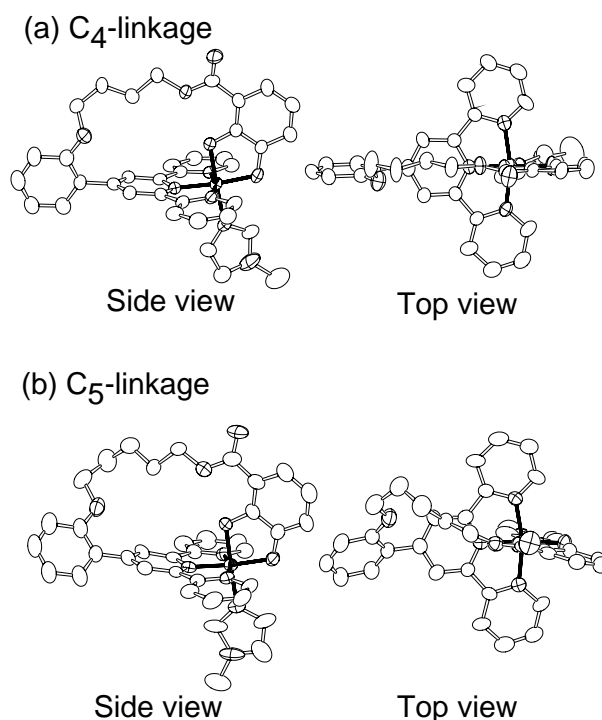


Figure 2. The X-ray structures of cobalt(III) complexes of the C<sub>4</sub>- and C<sub>5</sub>- linked ligands.



## VIII-K The Effects of the 2D Spin-Echo NMR Pulse Sequence on Homonuclear Spin Systems

Dipolar interactions for homonuclear spin systems are averaged out by magic-angle sample spinning (MAS). The 2D spin-echo NMR pulse sequence can reintroduce the influence of the homonuclear dipolar interactions into MAS powder signals.

### VIII-K-1 Novel Satellites in a Two-Dimensional Spin-Echo NMR Spectrum for a Homonuclear Spin-1/2 Pair in Rotating Solids

**KUWAHARA, Daisuke; NAKAI, Toshihito<sup>1</sup>; ASHIDA, Jun<sup>2</sup>; MIYAJIMA Seiichi**  
(<sup>1</sup>Tokyo Univ. Agric. Tech.; <sup>2</sup>Kyoto Univ.)

[*Chem. Phys. Lett.* **305**, 244 (1999)]

We found additional resonance lines on both sides of the center line along the F1 axis, when the 2D spin-echo pulse sequence was applied to a solid-state <sup>13</sup>C-<sup>13</sup>C spin system undergoing MAS. The lines are not attributed to well-known *J*-resolved doublets. To our surprise, the positions of the lines are determined by a quantity  $\kappa$ , which is a function of the sample spinning frequency and the difference of the isotropic chemical shifts. These lines were discovered for the first time as far as we know. The analysis based on a former publication was useful, but could not describe the general experimental scheme which employs an arbitrary value of  $t_1$  increment. An arbitrarily chosen  $t_1$  increment was applied for the experiments in the present study. The analytical representation for the 2D experiment is inevitable to explain the origin of the additional lines. We are now preparing such representation and the optimized simulation spectra.

# Equipment Development Center

## VIII-L Development of "IMS Machines"

The technical staff of the Equipment Development Center is partly engaged in planning, researching, designing and constructing "IMS machines." This machine, crowned with the acronym of the Institute for Molecular Science, is a high-tech experimental instrument, with emphasis on new technical idea and co-operative work with members inside and outside the Institute including those in industries. We collect suggestions of new instruments once every year from all of the members of IMS.

In this fiscal year, 1998, three project themes (1 through 3) were adopted as IMS machines. IMS machine project 4 (IMS machine 1997) was completed, and project 5 (IMS machine 1997) is under way.

1. **Thin Shaped Cryostat for Opto-magnetic Measurement**  
(proposed by Shinji IZUMIDA and Takuhiko KONDOH)
2. **Vibration Method Magnetometer**  
(proposed by Yuko HOSOKOSHI, developed by Nobuo MIZUTANI and Yuko HOSOKOSHI)
3. **Preparation and Transfer System for Ice-embedding Sample**  
(proposed by Toshio HORIGOME and Shinji HASEGAWA, developed by Mitsukazu SUZUI and Kazuhiro KOBAYASHI)
4. **Surface Profiler of Mirrors for High-Resolution Monochromator**  
(proposed by Toyohiko KINOSHITA, developed with Hisashi YOSHIDA, Toshio HORIGOME, and Shuji ASAKA)
5. **Off-Axis Paraboloid Polarizing Mirror for Far-Infrared Light**  
(proposed and developed by Hideyuki OHTAKE and Takayuki YANO)

### VIII-L-1 Surface Profiler of Mirrors for High-Resolution Monochromator

**YOSHIDA, Hisashi; HORIGOME, Toshio; ASAKA, Shuji; KINOSHITA, Toyohiko**

We are developing a measurement apparatus for a precise profiling of surfaces of optical elements which are necessary for constructing high-resolution monochromators in UVSOR facility. The outline of the present apparatus is shown in Figure 1. The light beam from the laser (L) incidents upon the sample under measurement (S), and the reflected light on the sample surface is detected by light detectors (D1 or D2). By measuring the direction of the reflected light, we can derive the surface shape of the sample.

We adopted glancing incidence geometry to ease measurement on plane, spherical and non-spherical mirrors with length of 10 cm to 1 m, which are often used in synchrotron radiation facility. In the present setup the position of the reflected light displaces in a relatively wide range during a measurement. To cope with this we used Y-Z translation stages with linear scales and 4-division photodiode detectors.

In order to determine the direction of the reflected light beam, we need to know the positions of arbitrary two points on the beam. One position is measured by detector D2, and the other is measured by detector D1 by detecting the light that is partly reflected by the beam splitter (B).

The present optical system is very sensitive to mechanical vibration, temperature change and air flow. We fixed the whole components on an air-suspended vibration-free table and covered them with a plastic booth in order to stabilize the apparatus.

The outer view of the apparatus is shown in Figures 2 and 3.

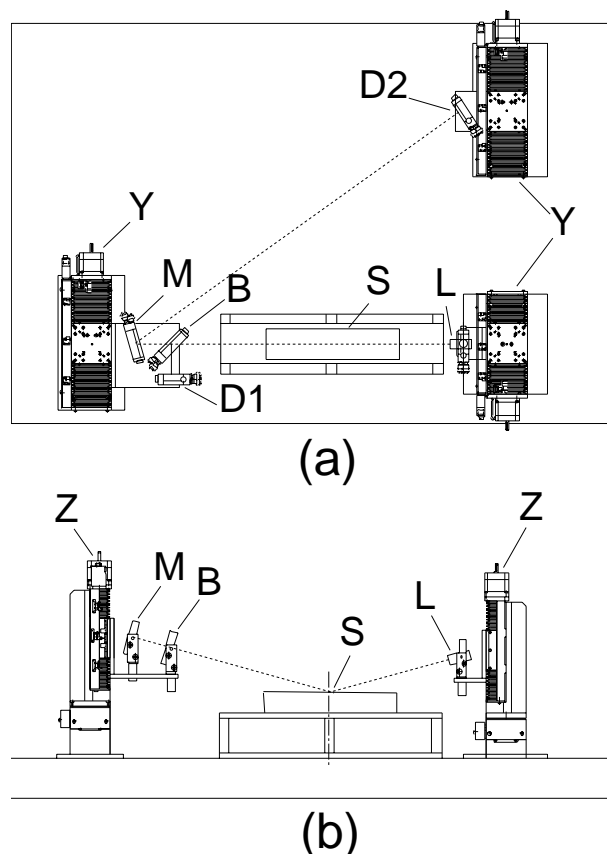


**Figure 1.** Design of the surface profiler. (a)Top view and (b)front view. L:Laser diode module, S:Sample mirror, B:Beam splitter, M:Mirror, D1 and D2:4-division photo diodes, Y and Z:Linear translation stages driven by stepping motors.

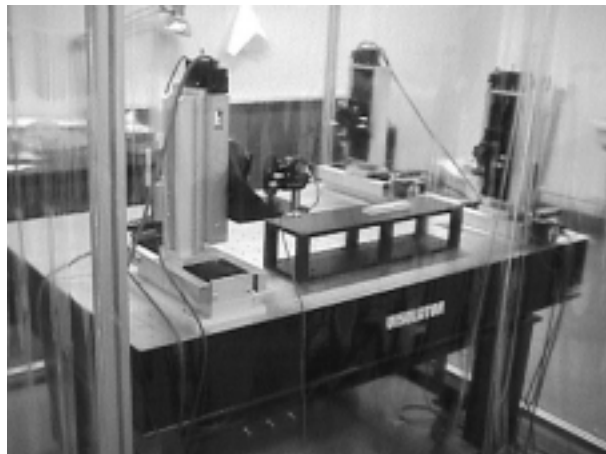


**Figure 2.** Surface profiler apparatus set up on a vibration-free table.



**Figure 3.** Driver for linear translation stage and host computer.

### VIII-L-2 Preparation and Transfer System for Ice-Embedding Sample

## VIII-M Development of New Laser Materials

### VIII-M-1 Amplification of Impurity-Associated Auger-Free Luminescence in Mixed Rubidium-Caesium Chloride Crystals under Core-Level Excitation with Undulator Radiation

MIKHAILIK, Vitalii B.<sup>1</sup>; ITOH, Minoru<sup>2</sup>; ASAKA, Shuji; BOKUMOTO, Yoshiho<sup>2</sup>; MURAKAMI, Junichi<sup>2</sup>; KAMADA, Masao

(<sup>1</sup>Lviv Franko State Univ.; <sup>2</sup>Shinshu Univ.)

We obtained results of experimental studies aimed at testing the amplification of impurity-associated Auger-free luminescence (275 nm band) in mixed rubidium-caesium chloride crystals under core-level excitation with undulator radiation. The emission features observed under the best collimation of the optical cavity, namely the enhancement of the peak intensity,

HORIGOME, Toshio; HASEGAWA, Shinji; KOBAYASHI, Kazuhiro; SUZUI, Mitsukazu

Spectral measurement of ice-embedding bio-molecules under ultra high vacuum is promising for detailed understanding of their electronic structure. Few experiments, however, have been succeeded due to technical difficulty, except for electron microscopy. We have a project to develop the preparation and transfer system for ice-embedding sample that is applicable to various spectral techniques.

Figure 1 shows our contrivance to enable the photoemission measurement on ice-embedding bio-molecules. It is made up by three parts for sample preparation with liq. ethane, cryogenic transferring of sample to a measurement chamber, and fast evacuation with the aid of a special inner valve that separates between moderate and ultra high vacuum. Eighty percent of the whole system has been constructed. This system will be situated and work at UVSOR beamline after completion.

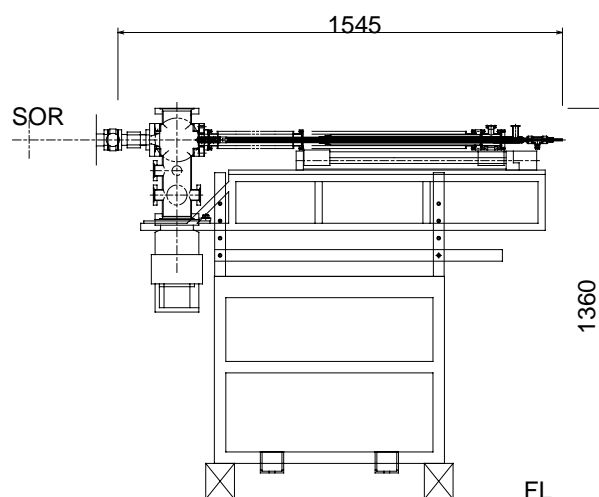


**Figure 1.** Preparation and transfer system for ice-embedding sample.

the sharpening of the emission spectrum and the shortening of the luminescence decay, suggest a possibility of the light amplification due to inverted population between the valence and 5pCs-impurity core states.

# Ultraviolet Synchrotron Orbital Radiation Facility

## VIII-N Development of the UVSOR Light Source

### VIII-N-1 Influence of Electron Beam Properties on Spontaneous Radiation from an Optical Klystron

HOSAKA, Masahito; YAMAZAKI, Jun-Ichiro; HAMA, Hiroyuki

[*Nucl. Instrum. Methods Phys. Res., Sect. A* **429**, 191 (1999)]

Spectrum of the radiation from an optical klystron is

very sensitive to the beam energy spread which is an important factor for the storage ring free electron laser. In order to make use of the spectrum for a measurement of the relative energy spread, we have investigated influences of the transverse beam property on the spectrum using a helical optical klystron on the UVSOR storage ring. From analysis of the experimental results, it has been found that the most important effect comes from inhomogeneous magnetic fields and a horizontal beam size.

## VIII-O Researches by the USE of UVSOR

### VIII-O-1 Nano-Second Desorption of Alkali Fluorides Excited by Synchrotron Radiation Pulses

KAMADA, Masao; TAKAHASHI, Naoshi; HIROSE, Sayumi<sup>1</sup>

(<sup>1</sup>Sumitomo Heavy Industry)

Desorption of the excited-state alkali atoms has been investigated on alkali fluoride crystals in the photon energy region of 20-75 eV, which includes the excitation energy for Li 1s-core excitons, Na 2p-core excitons, and valence excitations. The quantum yield of the excited-state alkali desorption was found to be comparable between valence and core-level excitations. Time response of desorption from LiF and NaF was also observed by using synchrotron radiation pulses. It was found that the time response consists of a nano-second component and slower one, indicating that the fast desorption is due to the lattice instability induced by electronic transition and the slow one is due to the thermal instability of surface defects.

### VIII-O-2 Photo-Induced Change in Semiconductor-Vacuum Interface of p-GaAs(100) Studied by Photoelectron Spectroscopy

KAMADA, Masao; MURAKAMI, Junichi<sup>1</sup>; TANAKA, Senku<sup>2</sup>; MORE, Sam Dylan; ITOH, Minoru<sup>1</sup>; FUJII, Yasuo<sup>2</sup>

(<sup>1</sup>Shinshu Univ.; <sup>2</sup>Osaka City Univ.)

The photo-induced change in the semiconductor-vacuum interface on GaAs (100) and Cs/GaAs(100) has been investigated by using a photoelectron spectroscopic technique with synchrotron radiation and a mode-locked Nd:YAG laser. Both Ga-3d and As-3d photoelectron peaks showed transient energy shifts under the laser irradiation without any spectral change. The amounts of the energy shifts were strongly dependent on the sample temperature and the laser photon flux. It was found that the dependence fits well to the theoretical curve derived from the surface photo-voltage effect based on the band bending scheme in the surface layer of the semi-

conductor.

### VIII-O-3 Electronic Structures of Organic Salts DMTSA-BF<sub>4</sub> Using Photoelectron Spectromicroscopy

HARUYAMA, Yuichi<sup>1</sup>; KINOSHITA, Toyohiko<sup>2</sup>; TAKIMIYA, Kazuo<sup>3</sup>; OTSUBO, Tetsuo<sup>3</sup>; NAKANO, Chikako; YAKUSHI, Kyuya

(<sup>1</sup>Himeji Inst. Tech.; <sup>2</sup>Univ. Tokyo; <sup>3</sup>Hiroshima Univ.)

The electronic structures of 1:1 charge-transfer organic salts DMTSA-BF<sub>4</sub>, where DMTSA is 2,3-dimethyltetraseleno-anthracene, have attracted the interest of many researchers because of the high electrical conductivity and metallic physical property.<sup>1)</sup> The photoemission study for DMTSA-BF<sub>4</sub> has not been performed so far since DMTSA-BF<sub>4</sub> is not large enough to carry out the ordinary photoemission experiments. We succeeded to measure the photoemission spectra for DMTSA-BF<sub>4</sub> using the photoelectron spectromicroscopy.

Figure 1 shows the photon energy dependence of the photoemission spectra for DMTSA-BF<sub>4</sub>. From the photon energy dependence of the photoionization cross-section, the atomic orbital characters of the observed spectral features are determined. The Se 4p states are located at ~1 eV, ~3 eV, and ~6 eV. The C 2p and F 2p states are located at ~8 eV. In our photoemission measurements, the clear Fermi edge was not observed. This suggests the importance of the electron correlation effect and/or one-dimensional nature for DMTSA-BF<sub>4</sub>. The photoemission spectra for DMTSA were also measured in order to compare the electronic structures for DMTSA-BF<sub>4</sub>. The Se 3d core level photoemission spectra did not show the chemical shift but the photoemission spectrum for DMTSA-BF<sub>4</sub> showed the tail at the higher binding energy side as compared with that for DMTSA. The difference of the electronic structures between DMTSA and DMTSA-BF<sub>4</sub> is discussed, based on the valence band and Se 3d core level photoemission results.

#### Reference

- 1) J. Dong, K. Yakushi, K. Takimiya and T. Otsubo, *J. Phys. Soc. Jpn.* **67**, 971 (1998).

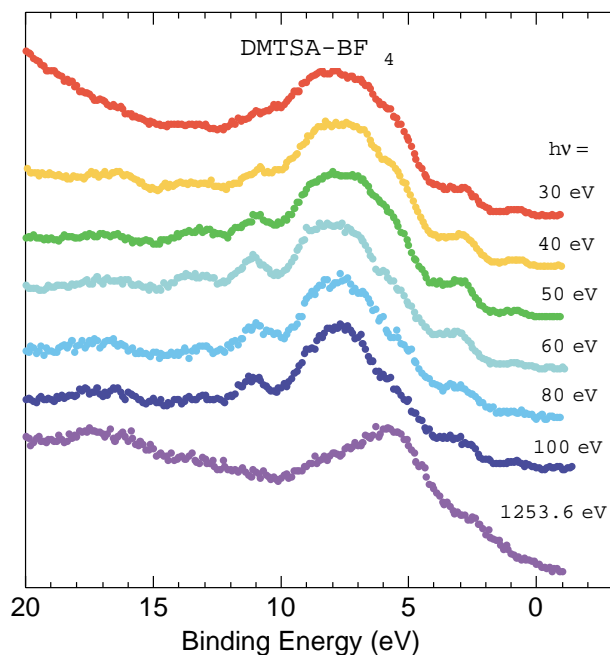


**Figure 1.** The photon energy dependence of the photoemission spectra for the organic salts DMTSA-BF<sub>4</sub>.

#### VIII-O-4 Photoemission Study of Si(111) Clean Surfaces at High Temperature Using Laser Annealing

HARUYAMA, Yuichi<sup>1</sup>; KINOSHITA, Toyohiko<sup>2</sup>; TANAKA, Shin-ichi  
(<sup>1</sup>Himeji Inst. Tech.; <sup>2</sup>Univ. Tokyo)

The electronic structures of Si (111) clean surfaces at high temperature have been studied using the photoemission spectroscopy. In the photoemission measurements, it is not easy to observe the electronic structures at high temperature because of the electric field used to anneal the sample to high temperature. By combining the laser annealing and the photoelectron spectromicroscopy, we demonstrate that the photoemission spectra at high temperature are easily obtained.

Figure 1 shows the temperature dependence of the photoemission spectra for Si (111) clean surfaces from room temperature to ~1200 °C. At room temperature, three surface states were observed at ~0.2, ~0.8 and ~1.8 eV. With increasing the annealing temperature, the surface state at ~0.8 eV disappears. The temperature dependence of the spectral features obtained in our measurements is essentially identical to that previously obtained by Yokotsuka *et al.*<sup>1)</sup> In addition, we found that the shift of the photoemission spectra was observed at ~0.2 eV higher binding energy side under 0.04~0.89 W laser irradiation. The shift at ~0.2 eV was also observed at the Si 2p core level photoemission spectra. With increasing the annealing temperature, the shift disappears at the laser power of 2.00 W. The observed shift indicates that the surface photovoltage effect<sup>2)</sup> is caused by the photocarrier, which is induced by the laser irradiation. The disappearance of the surface photovoltage effect may be caused by the metallic nature of the high temperature semiconductor.

#### References

- 1) T. Yokotsuka, S. Kono, S. Suzuki and T. Sagawa, *Solid State Commun.* **39**, 1001 (1991).
- 2) J. E. Demuth, W. J. Thompson, N. J. DiNardo and R. Imbihl, *Phys. Rev. Lett.* **56**, 1408 (1986).

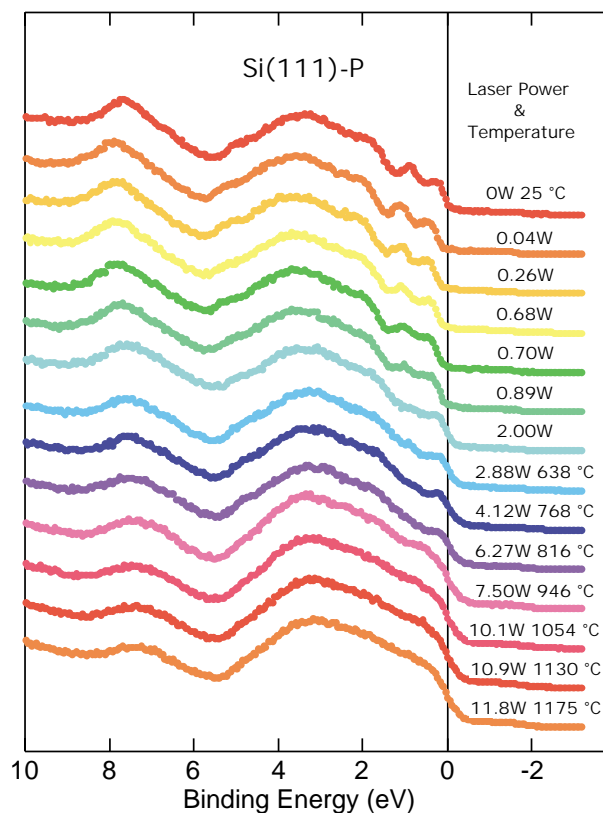


**Figure 1.** The temperature dependence for the Si (111) clean surface under laser irradiation.

#### VIII-O-5 Behavior of the “6eV Satellite” in Ni Thin Film Observed by Valence Band Photoemission

NATH, Krishna G.<sup>1</sup>; HARUYAMA, Yuichi<sup>2</sup>; KIMURA, Shin-ichi<sup>3</sup>; UFUKTEPE, Yüksel<sup>4</sup>; KINOSHITA, Toyohiko<sup>5</sup>  
(<sup>1</sup>NTT; <sup>2</sup>Himeji Inst. Tech.; <sup>3</sup>Kobe Univ.; <sup>4</sup>Univ. Cukurova, Turkey; <sup>5</sup>Univ. Tokyo)

[*J. Electron Spectrosc. Relat. Phenom.* **101-103**, 257 (1999)]

It is now well established that the electronic structures of thin films are interestingly different from those of bulk. In case of 3d-transition materials, this difference is directly related to the changing of *d*-band width, exchange integral and the magnetic moment with changing of the film thickness.<sup>1)</sup> In such situation, any correlation-induced peak in the photoemission, such as Ni-6eV satellite also shows some interesting and varied feature depending on the film thickness. Another important aspect, that has to be considered, is the hybridization effect between the film and substrate. Here, we report the Ni valence band photoemission result for different thickness films on ferromagnetic Co(001) in order to study the 6 eV satellite feature and the resonant effect on magnetic dichroism signal for satellite.

In Figure 1, we show a series of Ni-valence band photoemission spectra taken at  $h\nu = 67.2$  eV. The peak around the Fermi level is the main peak assigned by  $3d^9$  state. Another peak stayed around 6 eV is the satellite assigned as  $3d^8$  state. At  $h\nu = 67.2$  eV, the satellite peak shows resonance enhancement.<sup>2)</sup> The satellite peak positions for all films are indicated by dashed line. It is clear that satellite peak position is shifted to the higher binding energy for thicker films. The origins of this variation are the thickness dependent  $d$ -band width and the corresponding  $d$ - $d$  correlation effect. For thicker films, the large width of  $d$ -band pushes the satellite peak higher binding energy position. In Figure 2, we show the resonance effect on magnetic linear dichroism (MLD) for satellite peak where the sample is 8ML Ni grown on 10ML Co. After comparing with off-resonant result in Figure 2 (b), we found that the in-plane MLD signal for satellite shows resonant behavior.

#### Reference

- 1) W. Clemens *et al.*, *Solid State Commun.* **81**, 739 (1992).
- 2) C. Guillot *et al.*, *Phys. Rev. Lett.* **39**, 1632 (1977).

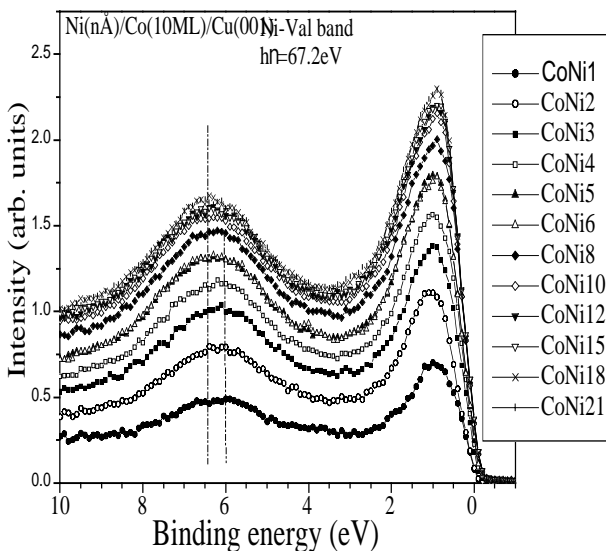


**Figure 1.** Ni-valence band photoemission spectra for Ni films of different thickness (1–21 Å). The peak around 6.5 eV is the satellite peak, which shows binding energy shift for thicker films as indicated by dashed line.

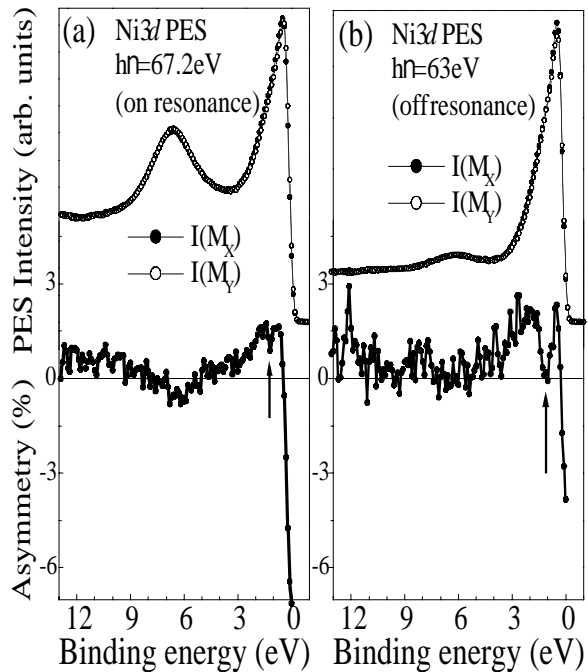


**Figure 2.** MLD for 8ML Ni on 10 ML ferromagnetic Co. In (a), MLD at on-resonance shows opposite trend for the main peak and the satellite peak. In (b), MLD at off-resonance where satellite shows weak MLD.

#### VIII-O-6 Magnetic Stability of Co-Film Grown on Oxygen-Rich Cu(001) Surface

NATH, Krishna G.<sup>1</sup>; HARUYAMA, Yuichi<sup>2</sup>; KINOSHITA, Toyohiko<sup>3</sup>  
(<sup>1</sup>NTT; <sup>2</sup>Himeji Inst. Tech.; <sup>3</sup>Univ. Tokyo)

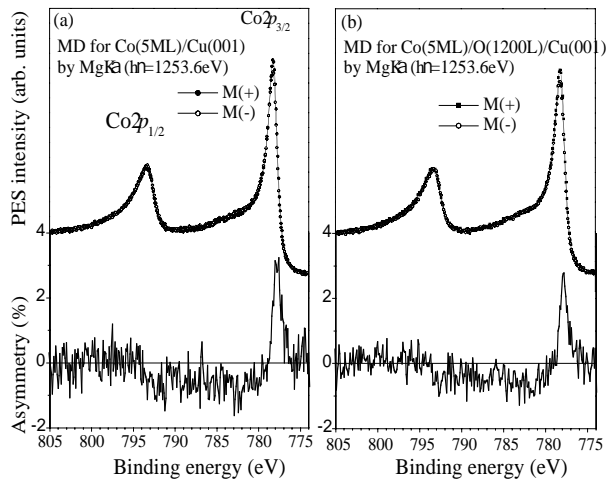
From the points of view of both technological application and fundamental research, it is a common intention to grow metal film on very clean surface (surface without any contamination). Using of clean substrate ensures the perfect crystalline growth, defect-free interface, and in the case of magnetic film, the magnetic stability. Oxygen is considered to be the most defined contamination from which we want to get ride of for getting good epitaxy. But oxygen can be also used as a surfactant<sup>1)</sup> (which promotes the layer-by-layer or well-shaped island growth). In the present study, we report the magnetic behavior of Co films grown on oxygen-rich Cu(001) substrate. We also checked the electronic structures, reconstruction phases, surfactant effect *etc.*

Figure 1 shows the magnetic dichroism (a technique to study the magnetism) results for two systems, (a) 5ML Co on clean Cu(001) and (b) 5ML Co on oxygen-rich Cu(001) surface. The oxygen-rich Cu, oxidized by 1200L oxygen, shows  $(\sqrt{2}\times\sqrt{2})R45^\circ$ -O reconstructed phase in LEED pattern. The 5ML Co film was then deposited on that oxidized Cu and was characterized by XPS and LEED. It was found that oxygen was segregated to Co surface and promotes to grow the  $c(2\times 2)$  reconstructed phase. The new state of oxygen on Co is the chemisorbed state. The interesting observation is that this reconstructed phase of Co also shows almost similar magnetic behavior to Co on clean Cu. The order

of dichroism signal is nearly same for both cases [as seen in Figure 1(a) and Figure 1(b)]. Therefore, it can be said that the large amount of oxygen on the Cu before Co deposition does not cause any negative effect on the magnetic (ferromagnetic phase) stability of Co film.

#### Reference

1) C. Tolkes *et al.*, *Phys. Rev. Lett.* **80**, 2877 (1998).



**Figure 1.** The MUDAD (magnetic dichroism in angular distribution by unpolarized light) for 5ML Co on fresh Cu [in (a)] and on oxidized Cu [in (b)]. The Co 2*p* peaks were measured for the two-magnetization directions. The almost same order of dichroism signal confirms the magnetic stability of Co films on oxygen-rich Cu.

#### VIII-O-7 Thickness Dependent Oxidization of Co Films and Observation of Different CoO Phases

NATH, Krishna G.<sup>1</sup>; HARUYAMA, Yuichi<sup>2</sup>; KIMURA, Shin-ichi<sup>3</sup>; KINOSHITA, Toyohiko<sup>4</sup>  
(<sup>1</sup>NTT; <sup>2</sup>Himeji Inst. Tech.; <sup>3</sup>Kobe Univ.; <sup>4</sup>Univ. Tokyo)

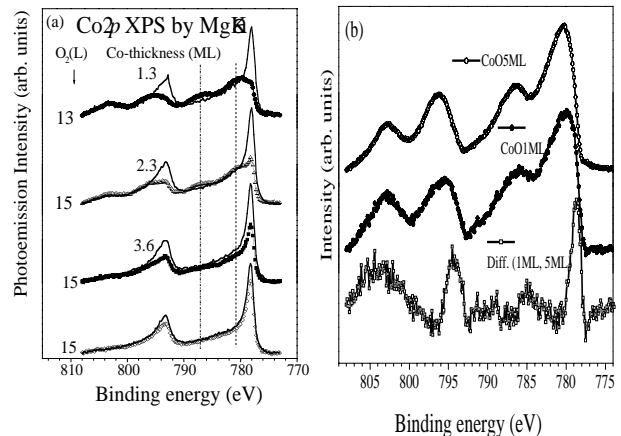
The bulk CoO is a well-known Mott insulator and shows strongly correlated nature. It is known that CoO can be also obtained by oxidization of bulk Co or Co-film. In case of bulk Co, the entire oxidization process is confined to only hcp structure, the only available phase at room temperature. By using artificial Co thin film, we can vary the oxidization process as growth behavior of Co on other metal, *e.g.* Cu(001), differs depending on the thickness. For example, Co films of less than 2ML on Cu show different sizes of island, whereas more than 2ML Co films grow in layer-by-layer mode and show fct (face center tetragonal) structure. We have studied the core level photoemission by growing CoO for different thickness of Co films.

Figure 1 (a), shows the Co2*p* photoemission spectra for clean and oxidized Co films, where the thickness of the Co is 1.3, 2.3, 3.6, and 5ML, respectively. The films were oxidized by almost same amount of exposure. In (a), spectra with symbols are for oxidized Co and solid lines are for clean ones. Peak at binding energy 778.0 is from elemental Co. Peak at 780.2 eV (dashed line) is assigned to be  $d^8\bar{L}$  ( $\bar{L}$  stands for ligand hole state) and the higher binding energy satellite (dotted-dashed line)

is assigned as the final state with a mixture  $d^9\bar{L}^2$  and  $d^7$  states on the basis of charge transfer (CT) theory<sup>1)</sup> for CoO. The results show that the thinner films are more reactive and show an early formation of CoO. In Figure 1 (b), the difference between the saturated CoO phase for 1ML and 10ML Co films is shown. It is noticed that the features for thinner film seem to be broader. Here we predict that the difference spectrum shown in this figure probably represents the 2D CoO phase, which is different from the bulk CoO phase.

#### Reference

1) K. Okada *et al.*, *J. Phys. Soc. Jpn.* **61**, 449 (1992)



**Figure 1.** Co2*p* XPS for different Co films. In (a), the solid spectra for elemental Co and spectra with symbol for oxidized Co films. In (b), the spectra of saturated CoO phase for 1ML and 5 ML Co films and their “difference spectrum.”

#### VIII-O-8 Satellite Structure Observed in 2*p* XPS of Co Thin Film

NATH, Krishna G.<sup>1</sup>; HARUYAMA, Yuichi<sup>2</sup>; KINOSHITA, Toyohiko<sup>3</sup>  
(<sup>1</sup>NTT; <sup>2</sup>Himeji Inst. Tech.; <sup>3</sup>Univ. Tokyo)

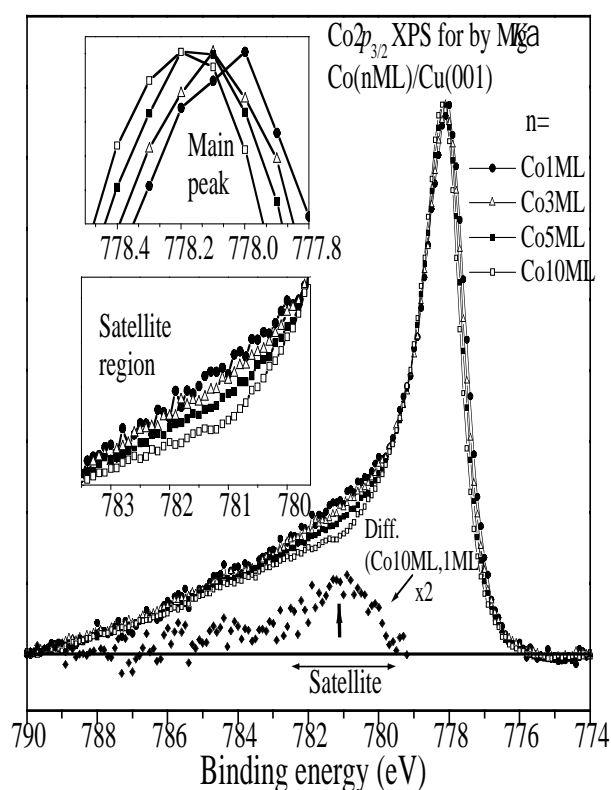
Satellite structures in the photoemission spectra for 3*d*-transition metals have been frequently reported for more than twenty years.<sup>1)</sup> The well-known example of the satellite structure is the 6*eV*-satellite in Ni valence band and core level photoemission.<sup>2)</sup> It is now established that the *d-d* interaction is the origin of the formation of satellite. This interaction might take a strong value at the surfaces and interfaces where the reduction of dimension exists along the surface normal. Therefore, we may expect the variation of satellite intensity if the thickness of the thin film system is considered to be a variable. At the same time, the hybridization between the film and the substrate might play an important role for observing the satellite.

Figure 1 shows the Co2*p*<sub>3/2</sub> XPS spectra for different thickness of Co films on the clean Cu(001) substrate. As shown in the figure, we observe a regular change in the four spectra for the both main peak (upper inset) and the satellite region (lower inset). In the case of 1 ML film, the film structure is considered not to be homogeneous, but island type. This situation may make different charge distribution (less *d*-hole) in the valence band at the Co-site. As a result, the chemical environment of the

atom from where the core electron is outgoing is changed. Therefore, the charge transfer process with the Cu and the Coulomb interaction may differ from these in thicker film. The situation causes the binding energy shift for the main peak. In case of satellite region (in lower inset), the intensity difference is also apparent. For 1 ML film, the states around 779.5-783.0eV binding energy is more intense than those in other films. This is shown clearly in the difference spectra between 1 ML and 10 ML films. The reasons for intense satellite in 1 ML film are the stronger *d-d* correlation and less hybridization with the substrate states.

#### References

- 1) S. Raaen, *Solid State Commun.* **60**, 991 (1986).
- 2) S. Hüfner *et al.*, *Phys. Lett. A* **51**, 299 (1975).



**Figure 1.**  $\text{Co}2p_{3/2}$  photoemission spectra for 1, 3, 5 and 10 ML Co films on Cu(001). **Upper inset.** The binding energy difference in the main peak. **Lower inset.** The intensity difference around the satellite region. This difference is clear in the "difference spectrum" of 1 ML and 10 ML (shown underneath of four spectra).

#### VIII-O-9 Design Study for a Varied-Line-Spacing Plane Grating Monochromator

SHIGEMASA, Eiji; TAKATA, Yasutaka; GEJO, Tatsuo

Recent conceptual and technological improvements to monochromators have enabled us to realize various studies on vibrational spectroscopy in the soft x-ray range (100~1000 eV), which contains the *K*-shell thresholds of chemically important elements like C, N, and O, even without the use of undulator radiation. At the UVSOR, there is only one monochromator for high

resolution spectroscopy in the photon energy region of interest (250~550 eV). A maximum resolving power of 4000 at 400 eV is achievable with this monochromator, but due to a little complicated scanning mechanism, it has difficulty maintaining such high resolution in the entire photon energy range. Design study for a new monochromator has recently been started in order to improve the situation. A Varied-line-spacing Plane Grating Monochromator (VPGM) has been chosen for this work. Thanks to the availability for high quality gratings and simple scanning mechanism, VPGM seems to be one of the most trustworthy monochromators to realizing high resolution in the soft x-ray range. Figure 1 shows a layout of the optical elements of the present VPGM. The resolution of this monochromator was studied by ray-tracing simulation as well as analytical estimation. This study shows that a resolving power of more than 5000 is achievable over the energy range from 250 to 550 eV with one single grating having the groove density of 1000 l/mm.

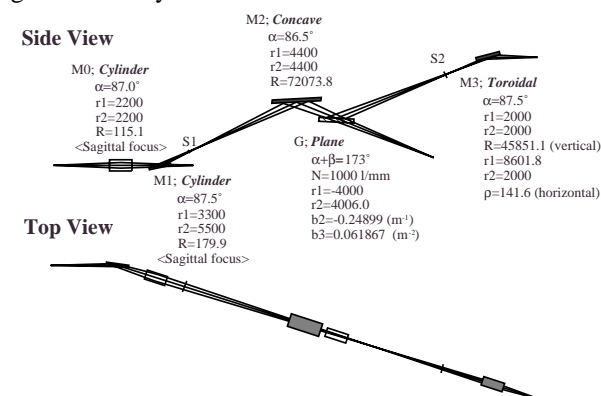


**Figure 1.** Schematic layout of the designed monochromator.

#### VIII-O-10 Photodissociation of Ozone in the K-Edge Region

GEJO, Tatsuo; OKADA, Kazumasa<sup>1</sup>; IBUKI, Toshio<sup>2</sup>; SAITO, Norio<sup>3</sup>  
(<sup>1</sup>Hiroshima Univ.; <sup>2</sup>Kyoto Univ. Edu.; <sup>3</sup>ETL)

[*J. Phys. Chem. A* **103**, 4598 (1999)]

Ozone is one of the most important molecules in chemistry since ozone in the stratosphere absorbs UV light emitted from the sun and prohibits humanity from the exposure by the UV light. We have investigated the photochemistry and photodissociation dynamics of Ozone in *K*-edge region with angle-resolved time-of-flight apparatus for the first time. The  $\beta$  values and kinetic energy distributions were calculated from simulation of the TOF spectra obtained. The  $\beta$  value of  $\text{O}^+$  at an excitation energy of 529.0 eV is  $-0.7$ , which is consistent our previous assignment that the 529 eV band comes from the  $\pi^*(2b_1) \leftarrow 1s(2a_1)$  transition. In contrast to this, the  $\beta$  value at an excitation energy of 535.7 eV is  $-0.3$ . This implies that the transition moment does not lie perpendicular to the molecular plane and that this band should be mixed by more than two transitions. They are consistent with the previous assignments<sup>1)</sup> that the 529 eV band is the  $\pi^* \leftarrow \text{O}_T(1s)$  resonance excitation and that the 536 eV band is mainly

consisted of two transition, the  $\pi^*(2b_1) \leftarrow O_C(1s)$  and the  $\sigma^*(7a_1) \leftarrow O_T(1s)$ .

#### Reference

1) T. Gejo, K. Okada and T. Ibuki, *Chem. Phys. Lett.* **277**, 497 (1997).

### VIII-O-11 Infrared Magnetic Circular Dichroism of Strongly Correlated 4f Electron Systems with Synchrotron Radiation

KIMURA, Shin-ichi

[*Jpn. J. Appl. Phys., Part 1* **38**, 392 (1999).]

Magnetic circular dichroism (MCD) experiment in the infrared region using synchrotron radiation has been done for the first time. Since the off-axis component of the synchrotron radiation is circular polarization in itself, a MCD spectrum in wide energy range can be measured easily by using the infrared synchrotron radiation. The experimental method is suitable for the investigation of strongly correlated electron systems because the electronic structure, which is made by magnetic many-body interactions, is located in the wide energy region near the Fermi level.

### VIII-O-12 Optical Conductivity of the Kondo Insulator YbB<sub>12</sub>: Gap Formation and Low-Energy Excitations

OKAMURA, Hidekazu<sup>1</sup>; KIMURA, Shin-ichi; SHINOZAKI, Hidenori<sup>1</sup>; NANBA, Takao<sup>1</sup>; IGA, Fumitoshi<sup>2</sup>; SHIMIZU, Naoya<sup>2</sup>; TAKABATAKE, Toshiro<sup>2</sup>

(<sup>1</sup>Kobe Univ.; <sup>2</sup>Hiroshima Univ.)

[*Phys. Rev. B* **58**, R7496 (1998)]

[*Jpn. J. Appl. Phys. Series 11*, 85 (1999)]

[*Physica B* **259-261**, 317 (1999)]

Optical reflectivity experiments have been conducted on single crystals of the kondo insulator YbB<sub>12</sub> in order to obtain its optical conductivity,  $\sigma(\omega)$ . Upon cooling below 70 K, a strong suppression of  $\sigma(\omega)$  is seen in the far-infrared region, indicating the opening of an energy gap of ~25 meV. This gap development is coincident with a rapid decrease in the magnetic susceptibility, which shows that the gap opening has significant influence on magnetic properties.